Wind and Structures, *Vol. 30, No. 4 (2020) 339-366*
DOI: https://doi.org/10.12989/was.2020.30.4.339

Flow-conditioning of a subsonic wind tunnel to model boundary layer flows

Tarek Ghazal, Jiaxiang Chen, Moustafa Aboutabikh, Haitham Aboshosha* and Sameh Elgamal

Civil Engineering Department, Ryerson University, 350 Victoria, St. M5B 2K3, Toronto, Canada

(Received January 26, 2019, Revised November 21, 2019, Accepted January 31, 2020)

Abstract. This study aims at modeling boundary layers (BLs) encountered in sparse and built environments (i.e. open, suburban and urban) at the subsonic Wind Tunnel (WT) at Ryerson University (RU). This WT has an insignificant turbulence intensity and requires a flow-conditioning system consisting of turbulence generating elements (i.e., spires, roughness blocks, barriers) to achieve proper turbulent characteristics. This system was developed and validated in the current study in three phases. In phase I, several Computational Fluid Dynamic (CFD) simulations of the tunnel with generating elements were conducted to understand the effect of each element on the flow. This led to a preliminary design of the system, in which horizontal barriers (slats) are added to the spires to introduce turbulence at higher levels of the tunnel. This design was revisited in phase II, to specify slat dimensions leading to target BLs encountered by tall buildings. It was found that rougher BLs require deeper slats and, therefore, two-layer slats (one fixed and one movable) were implemented to provide the required range of slat depth to model most BLs. This system only involves slat movement to change the BL, which is very useful for automatic wind tunnel testing of tall buildings. The system was validated in phase III by conducting experimental wind tunnel testingof the system and comparing the resulting flow field with the target BL fields considering two length scales typically used for wind tunnel testing. A very good match was obtained for all wind field characteristics which confirms accuracy of the system.

Keywords: Wind Tunnel (WT); flow conditioning system; Boundary Layer (BL); turbulence; Computational Fluid Dynamics (CFD); Large Eddy Simulation (LES)

1. Introduction

Wind is the main loading case for tall buildings. Design codes such as NBCC (2015), ASCE (2016), Eurocode (2010) and AS/NZs (2010) can be used for load evaluation however, the codes have limitations with respect to the building height, shape and surrounding configuration. Wind tunnel (WT) and CFD can overcome these limitations. WTs have been used in studying tall buildings since mid-sixties when Alan Davenport investigated wind effects on the old-world trade center (Isyumov 2012). Afterwards, WTs were used extensively to study the behavior not only for tall buildings (Perera 1978, Ishizaki and Nishimura 1992, Li *et al*. 2004, Irwin *et al*. 2012, Tamura *et al*. 2013, Holmes 2014, Kim *et al*. 2015, Tamura *et al*. 2017, Hui *et al*. 2017, Li *et al*. 2018), but also for low-rise buildings (Ho *et al*. 1990, Kim *et al*. 2013), bridges (Davenport 1961, Tanaka and Davenport 1983) and flexible energy infrastructure (Loredo-Souza and Davenport 1998, 2001, 2002, Piccardo and Solari 1998, Nguyen *et al*. 2015a, 2015b, Aboshosha *et al*. 2016, Elawady *et al*. 2017, Jubayer and Hangan 2016).

CFD is relatively new for load evaluation of tall buildings when compared to WT. Although CFD can lead to faster results, it still needs further verifications and validations. A new High-Performance Computing HPC CFD code capable of simulating tall building aerodynamics and predicting wind-induced responses is currently being developed by the research team at Ryerson University RU.

This code needs to be validated which will be done using the subsonic WT available at RU. This subsonic WT has a closed loop with a test cross section of approximately 1m x 1m. The wind tunnel is suitable for smooth flow (i.e. aerospace applications) with a maximum turbulence intensity of 0.5% (Carroll 2017, Barcelos 2015). This is significantly less than the turbulence intensities encountered by tall buildings which are engulphed in atmospheric Boundary Layer (BL) (ESDU 2001-2002). It is essential for accurate wind load-evaluation to properly simulate the BL with the proper turbulence (Davenport 2002, Cermak 2003). This study focuses on designing a system to enable the subsonic WT at RU to model proper BL flows for different terrain conditions (i.e., open, suburban and urban).

Most BL WTs have a contraction zone to streamline the flow at the upstream followed by a flow-conditioning system to generate the target turbulence. Typically, this system consists of spires, barrier(s) and roughness blocks. There are extensive studies in the literature related to generating proper BLs in WTs. Systems used to generate the BL can be categorized under three categories: (i) Category 1 - Passive system with spires, barriers and blocks, (ii) Category 2 - Passive system with grids only and (iii) Category 3 - Active system with a dynamic grid (moving louvers) and blocks.

Researchers started to use Category I (Passive system with spires, barriers and blocks) after the early studies by Davenport (1961) and Counihan (1969a, 1969b, 1973). The system which is referred to as Counihan system, generates a proper BL with near-zero pressure gradient and is shown in Fig. 1. This figure represents a photo taken from inside the BL WT at University of Western Ontario and shows the

*Corresponding author, Assistant Professor
E-mail: habo@ryerson.ca

ISSN: 1226-6116 (Print), 1598-6225 (Online)

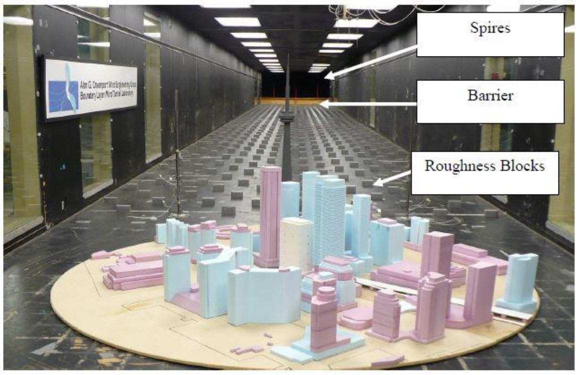

Fig. 1 Category I (Counihan System) of generating Proper Turbulence, Photo from BLWT

3 components of the system (spires, barrier and roughness blocks). Robins (1979), used Counihan's system to determine the length of the streamwise fetch necessary for the flow development. The study concluded that a fetch length of 12 to 15 times the BL height is typically needed to achieve a well-developed BL (naturally grown zero pressure gradient BL). This can be a challenge for WTs with limited space such as the tunnel at RU.

Inspired by Counihan (1969) and Robins (1979) Farell and Iyengar (1999) succeeded to simulate urban BL using quarter-elliptic constant wedge angle spires, a castellated barrier and roughness elements in a staggered arrangement. Irwin (1981) characterized the flow generated from Counihan system and developed semi-analytical design equations for the spires depending on the target scale, tunnel dimensions, and target BL. These equations were validated by Irwin (1981), and others (e.g., De Paepe *et al*. 2016) to be useful in achieving proper BLs. However, the equations typically lead to a BL with a limited acceptable depth (i.e., ~ 40% of the tunnel height, e.g., ~ 43 cm out of 108 cm for the WT at RU), which is not adequate for studying tall building aerodynamics at a suitable scale.

Cheng and Castro (2002) and Schultz *et al*. (2005) conducted wind tunnel studies for BLs resulting from multiple upstream terrains. Salizzoni *et al*. (2008) studied the interaction between large scale (i.e buildings) and small-scale (i.e., street-level obstacles and elements on the facades and roofs) roughness and their effect on the flow in the urban BL. They used spires similar to Counihan and Irwin systems, but utilized multiple barriers and mounted the roughness blocks (small scales) on the top of the barriers, with the aim of modeling parallel canyons in the built-environment. They found a modest effect of the added small-scale roughness when the large-scale obstacles are closely packed (increase the turbulence intensities and momentum transfer). Kozmar (2011) re-designed the spires of Counihan ignoring the tunnel height, but truncated the part above the tunnel height (above 1.7 m), to fit inside the tunnel. This led to spires coving the entire height of the tunnel, which is not the case for the original Counihan or Irwin's system (Counihan 1969, Irwin 1981). A highly calibrated BL with a depth covering ~ 95% of the tunnel height (1.7 m out of 1.8 m) was achieved by this, which is very useful for tunnels with low height such as the WT at RU.

Varshney (2012) conducted a parametric study on the passive turbulence generating elements (spires, barrier, roughness blocks) in addition to slots at the nozzle of the wind tunnel upstream of the spires and managed to generate all major types of BLs. The study showed that to generate a deep BL extending to a larger portion of the tunnel height (which is the target for the WT at RU), additional turbulence generating element (i.e., slots with variable width) is needed beside the typical system of spires, roughness blocks and barrier. Shojaee *et al*. (2014) used an aerospace WT to simulate BL. Because the tunnel had a shorter fetch length, a system of custom-designed spires was employed at the inlet followed by cubical surface roughness elements to create the proper BL for three main exposures. Aly *et al*. (2011) used a system of airfoils, and/or adjustable plank mechanism with or without grids to simulate hurricane winds in the open jet facility wall of wind (i.e., WoW) at Florida International University. They achieved proper BLs and identified acceptable range of model location and size to fit within the BLs. They found out that the model height should be within 1/3 of the generated BL thickness to allow for accurate pressures on the roof. This 1/3 constrain results from the freedom of the air movement in the open jet where no bounding walls exist. Mooneghi *et al*. (2014) used WoW facility to generate different BLs employing triangular spires, floor roughness elements to examine the uplifting of concrete roof pavers for low rise buildings. Pires *et al*. (2013) generated an open terrain BL on a short tunnel (i.e., 465 × 465 × 1200 mm) utilizing turbulence generating elements: spires, screens (grid) and floor mats individually and in-combinations. The results showed that the spires and screen achieved proper BL with least occupied tunnel area suitable for tunnels with short test chambers. De Paepe *et al*. (2016) generated the BLs using 2 systems: (i) Truncated Counihan ellipses, a grooved barrier and roughness elements and (ii) Truncated Irwin spires followed by roughness elements. Both truncated systems led to proper deep BLs (i.e., up to 80% of the tunnel height), but Irwin's spires achieved slightly better results.

Category 2 of the turbulence generating systems (i.e., employing passive grids) was utilized by many researchers in studying wind effects on sections of bridges and buildings. This system is capable for generating a kind of uniform turbulence intensity suitable for simulating a portion of the BL. Although, this is enough to study aerodynamics of the cross section of a building or a bridge, it is not suitable to study an entire building engulphed in BL (Davenport 1961, Ishizaki and Nishimura 1992, ESDU 2001, Han *et al*. 2010, Ge *et al*. 2014; Sun *et al*. 2017, Liu *et al*. 2017) investigated the turbulent parameters (i.e., turbulence intensity and wind speed) generated by using two different grids with different dimensions (i.e., width, thickness and height). The distance required for flow stabilization as well as obtaining a uniform turbulence intensity for both grids were determined. Vita *et al*. (2018) employed grids to generate proper turbulence and investigated the effect of tunnel expansion (diffusing) on the turbulence characteristics.

Table 1 Summary of previous studies on modeling BL at WTs

Type	Study	Application	Main Comments
Category I: passive system with spires, barrier and roughness blocks	Robins (1979)	N/A* (BL simulation)	Modeled consisted of Lego bricks for the rural case, wooden blocks for the urban terrain and a barrier wall.
	Perera (1978)	Tall, slender structures	Used a castellated barrier, quarter elliptical shaped vortex generators and roughness elements to model BL.
	Tanaka and Davenport (1983)	Golden gate bridge	Three terrain exposures were studied, that represents the bridge site and the open ocean fetch to westward.
	Ho *et al*. (1990)	Low rise buildings	Generated boundary layer using computer-controlled roughness elements and three 1.5 meters spires. (suburban and open terrains).
	Ishizaki and ishimura (1992)	Tall building	Generated uniform and turbulent flows with Turb. Int. =2% (smooth) and 20% (sub urban), respectively.
	Farell and Iyengar (1999)	N/A* (BL simulation)	Simulated urban BL through using quarter-elliptic, constant wedge angle spires, a castellated barrier wall and roughness elements.
	Loredo-Souza and Davenport (1998, 2001, 2002)	Transmission lines	For smooth surface, vertical flat plates in a staggered arrangement were used. For rough surfaces 2D rib type roughness was used.
	Cheng and Castro (2002)	Flow over smooth and rough surfaces.	Conducted wind tunnel tests to determine the spectral model of across wind forces on tall buildings. Urban BL was modelled.
	Li *et al*. (2004)	Tall buildings	Used sharp edged wooden cube to model urban BL.
	Schultz *et al*. (2005)	Urban BL	Used spires, roughness blocks, square bars and roughness elements to generate BL.
	Salizzoni *et al*. (2008)	Neutral turbulent BL	Modeled rural, suburban and urban terrains through using castellated barrier wall, vortex generators and surface roughness elements.
	Kozmar (2011)	N/A* (BL simulation)	Generated suburban and open terrain profiles
	Aly *et al*. (2011)	Different wind profiles	Simulated various BLs and found out that barriers and roughness blocks had the most significant effect on wind characteristics.
	Varshney (2012)	N/A* (BL simulation)	Simulated urban area using spires and roughness blocks.
	Irwin *et al*. (2012)	High rise building	Used different sized blocks, spires and barriers. Simulated suburban BL.
	Kim *et al*. (2013)	Low rise building	Utilized truncated spires with roughness blocks to simulate various BLs in short aeronautical wind tunnel.
	Shojaee *et al*. (2014)	High-rise buildings	Simulated ABL for aeronautical WT using screens, spires and a carpet for nearly flat terrains.
	Pires *et al*. (2013)	N/A* (BL simulation)	Simulated urban terrains using spires and roughness blocks to model the BL.
	Tamura *et al*. (2013)	Super tall building	Simulated urban terrains using spires and roughness blocks to model the BL.
	Mooneghi *et al*. (2014)	Concrete roof pavers	Used spires, floor roughness elements to generate BL for suburban terrain.
	Kim *et al*. (2015)	High-rise building	The flow represented an urban wind exposure through
	Jubayer and Hangan (2016)	Solar photovoltaic (PV) panels	Modeled open terrain roughness profiles.
	De Paepe *et al*. (2016)	N/A* (BL simulation)	Suburban ABL simulation using two different techniques and compared their results with international codes.
	Li *et al*. (2018)	Super tall building	Generated ABL using spires and floor roughness elements. Four terrain types were studied with different roughness lengths.
	Tamura *et al*. (2017)	Super tall buildings	Simulated urban area
Category II: Passive	Liu *et al*. (2017)	Turbulent field parameters	Studies BL resulting from only 2 grid types, but concluded that other factors (such as roughness blocks) can affect the turbulence.
	Cui and Caracoglia (2017)	Tall buildings	Generated BL using a grid but in a small-scale wind tunnel.
	Vita *et al*. (2018)	Partial BL Modeling	Studied the effect of an expansion test section for aeronautical WT on the turbulence characteristics.
Category III: Active	Jubayer *et al*. (2016)	Low rise building	Wind characteristics were simulated using mechanical louvers, but the roughness elements were not used.
	Jubayer and Hangan (2018)	Topography model (Complex terrain)	Three critical local BLs result at wind direction of (120,180 and 330) due to the complex surrounding effect.

Notes:
* refers to no application other than the BL simulation and flow characterization

Category 3 of the turbulence generating systems (i.e., with active elements) typically consists of dynamic louvers at the inlet with/without roughness blocks. This system is typically utilized in wide wind tunnel with short fetch length to rapidly induce target turbulence. For example, Ma *et al*. (2013) used multiple fans and vibrating airfoils system to study the aerodynamic behavior of a streamlined box girder. Jubayer *et al*. (2016) and Jubayer and Hangan, (2018) used a system of louvers with turning vanes to impose turbulence at the inflow to characterize the wind field in complex terrains.

Table 1 summarizes the literature on modeling BL at WTs and shows the category of each of the studies and typical applications. As shown in the table most of the studies belong to category I or II (passive with spires, barrier and roughness blocks or passive with grid only). Those studies provide a very good insight about the effect of each of the turbulence generating elements on the resulting BL. These insights are utilized here in the current study to design a flow-conditioning system to generate target BLs at the subsonic WT at RU, with suitable depth to allow for testing of tall buildings. This design and validation were obtained in three phases, where phase I focused on the understanding the effect of each turbulence generating element on the flow and resulted in a preliminary design, phase II focused on refining the design to achieve target BLs, and phase III focuses on the validation. First two phases utilize the Computational Fluid Dynamic (CFD) simulations of the WT with the turbulence generating elements to characterize the flow, while phase III utilizes experimental wind tunnel testing.

The manuscript is divided into 6 sections. Section 1 (this section) presents a review of the literature on BL modeling at WTs and a layout of the manuscript. Section 2 discusses details about the employed CFD model, details of the WT at RU and how the flow field obtained from the CFD is analyzed. Section 3 focuses on phase I where the behavior of BLs resulting from altering the turbulence generating elements was investigated. This part of the study led to a preliminary design of flow conditioning system where the BLs are generated using spires with movable barriers (i.e., slats). Section 4 focuses on phase II of the system design, where the system was refined to generate BLs for the typical range of terrain exposures (i.e., open, suburban, urban) using a system of dual-slats. Section 5 focuses on Phase III in which experimental wind tunnel testing of the system was conducted to validate the system. Section 6 summarizes the findings and conclusions.

2. CFD Modeling

This section describes the current wind tunnel at Ryerson University, followed by details of the CFD modeling and flow analysis.

2.1 Tunnel dimensions

Ryerson University currently operates a large subsonic, closed-loop WT for aerospace applications which is shown Fig. 2(a). This wind tunnel was refurbished in 2014/2015 to improve runtime and flow quality (Barcelos 2015, Carroll 2017). The tunnel is equipped with a large fan that pushes air at the north side of the tunnel as shown in Fig. 2(a). The pushed air passes through turning vanes and then through a contraction zone to streamline the flow at the south side before the test section. The test section has dimensions of 91 x 91 cm, with very smooth flow (Turbulence intensity of 0.5% or less). Located behind the test section is a diffuser zone with dimensions varying from 91 x 91 cm to 108 x 108 cm.

It is planned to utilize the south section of the tunnel to simulate BL flows (from the contraction zone to the diffuser zone) as marked in Fig. 2(a). The original test section right after the contraction is utilized to generate the turbulence, while the diffuser zone is utilized to characterize the flow and test building models. As discussed earlier, the study focuses on designing the flow conditioning system utilizing CFD. All thee CFD simulations focused on the south portion of the tunnel (contraction to the diffuser) as shown in Figure 2b. It is worth mentioning that the computational domain was extended for 0.5 meters behind the diffuser to remove the effect of local outflow boundary condition.

2.2 Computational modeling methods and parameters

Commercial CFD package (Fluent 18.1) is utilized to solve the Large Eddy Simulation (LES) defined by Eq. (1). Dynamic Sub-Grid scale model by Smagorinsky (1963) and Germano *et al*. (1991) is used to account for the turbulence. Parameters used to handle flow quantities as well as the solution technique are summarized in Table 2.

$$\begin{aligned}
&\frac{\partial \overline{u_i}}{\partial x_i} = 0\\
&\frac{\partial \overline{u_i}}{\partial t} + \overline{u_j}\frac{\partial \overline{u_i}}{\partial x_j} = -\frac{1}{\rho}\frac{\partial \overline{P}}{\partial x_i} + \frac{\partial}{\partial x_j}(-\tau_{ij} + 2\nu\overline{S_{ij}})\\
&\tau_{ij} = \overline{u_i u_j} - \overline{u_i}\,\overline{u_j}\\
&\overline{S_{ij}} = \frac{1}{2}\left(\frac{\partial \overline{u_i}}{\partial x_j} + \frac{\partial \overline{u_j}}{\partial x_i}\right)\\
&\tau_{ij} - \frac{1}{3}\delta_{ij}\tau_{kk} = 2\nu_e\overline{S_{ij}}\\
&\nu_e = (C_s.\Delta)^2\left(2\overline{S_{ij}}\,\overline{S_{ij}}\right)^2
\end{aligned} \tag{1}$$

Where i=1,2,3 corresponds to x, y and z directions respectively. The over bar represents the filtered quantities, u_i,p,t,τ_{ij} and ν represent fluid velocity, pressure, time, the SGS Reynolds stress and molecular viscosity coefficient, respectively. S_{ij},V_e,Δ,C_s represent strain rate tensor, eddy viscosity, grid size and Smagorinsky constant which is determined instantaneously based on the dynamic model respectively (*Germano et al*. 1991). δ_{ij} represents Kronecker delta.

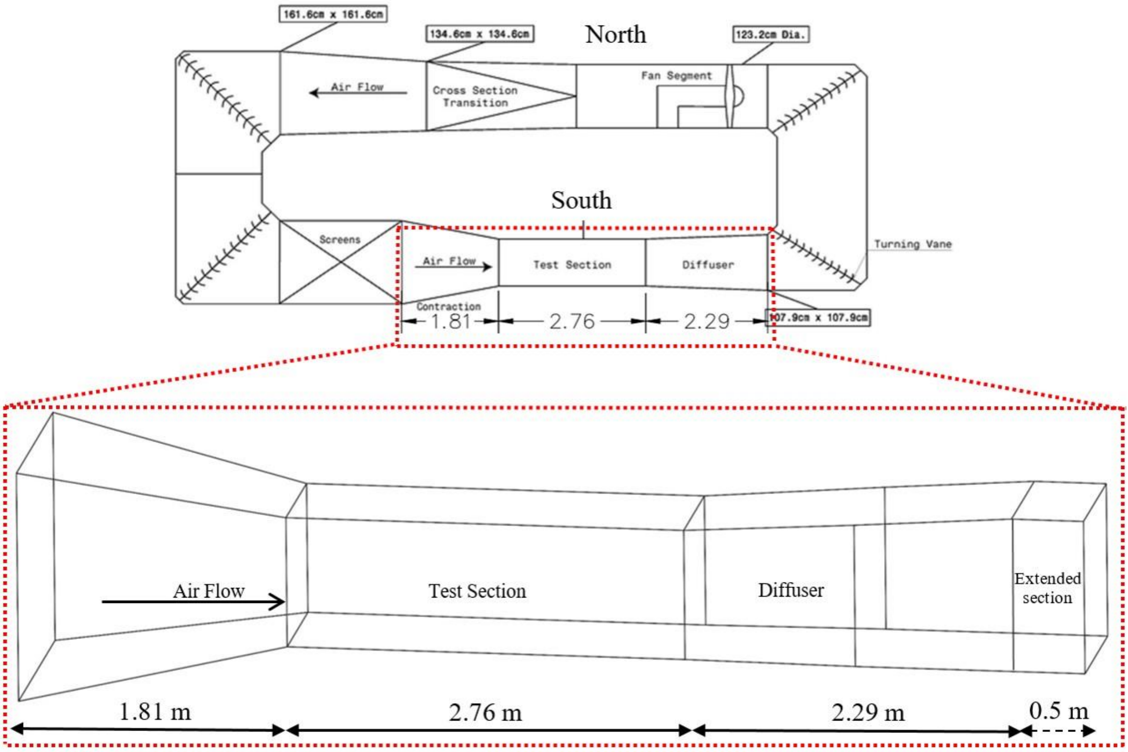

Fig. 2 Wind tunnel layout and computational model: (a) subsonic wind tunnel at RU (Barcelos 2015), (b) computation model of wind tunnel test section

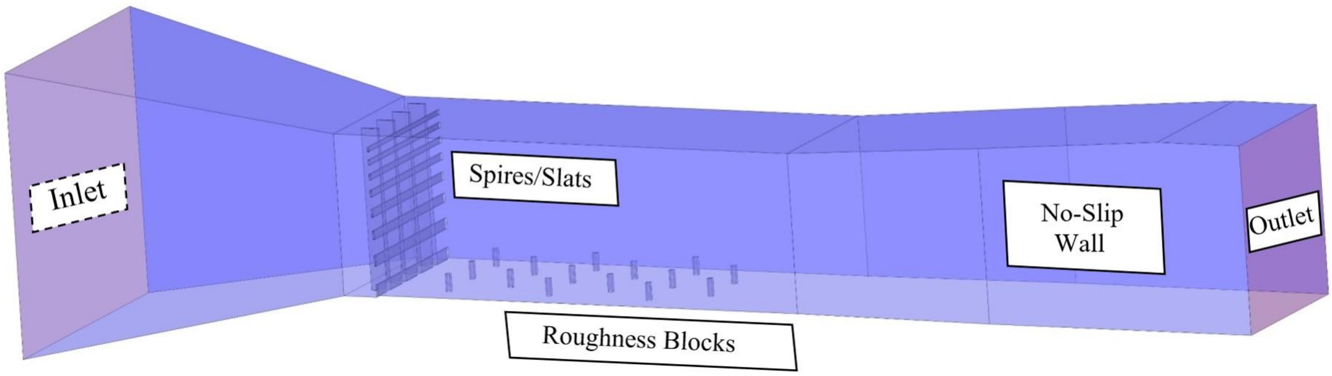

Fig. 3 Computational domain and boundary condition

Table 2 LES parameters

Parameter	Type
Time discretization	Bounded second order implicit
Momentum discretization	Bounded central differencing
Pressure discretization	Second order
Pressure-velocity coupling	Simple
Under relaxation factors	0.75 for flow variables only

Fig. 3 shows the computational domain with the boundary conditions utilized. The domain consists of inlet, outlet, walls, grounds as well as turbulence generating elements. Walls, ground as well as turbulence generating elements were classified as non-slip walls while the inlet is modeled as uniform inflow with a mean velocity of 10 m/s.

In order to maintain solution convergence as well as accuracy, the Courant-Friedrich-Lewy (CFL) number of less than 1 was maintained in all simulations. A limited-grid independence study was conducted utilizing 2 grids. Figure 4 shows the general grid details of the overall domain while Fig. 5 shows mesh details summ of the turbulence generating elements of the two grids. Table 3 arizes the properties of the employed grids, time step and simulation time utilized. The grids were conducted for a selected case where the flow was conditioned using spires with multiple horizontal slats (which will be explained later in section 3).

2.3 Analyzing CFD results

Flow field in terms of velocities was obtained and stored from the CFD simulations. Longitudinal velocities (u) in x-direction were recorded at 4 longitudinal intervals (i.e.,

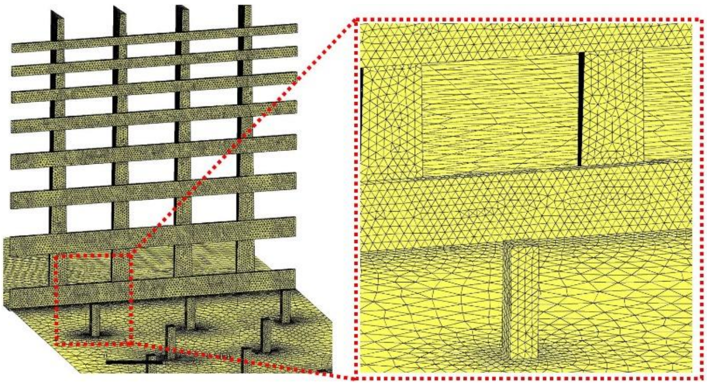

Fig. 4 General grid details : (a) Overall view of turbulence generators, (b) Close up of turbulence generators

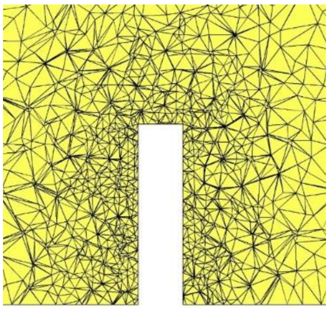

(a) Grid 1 roughness block

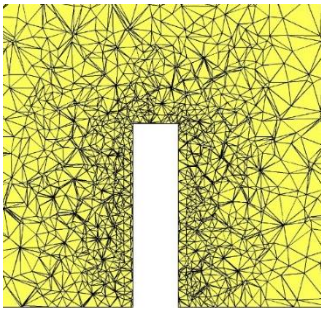

(b) Grid 2 roughness block

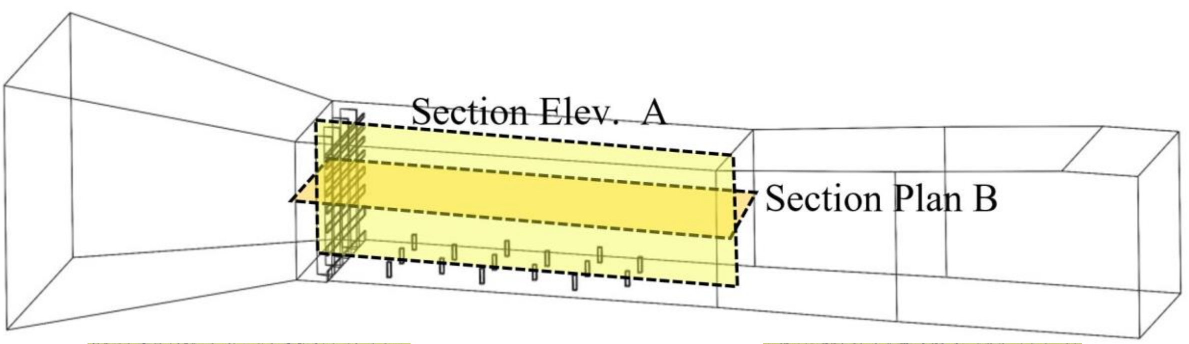

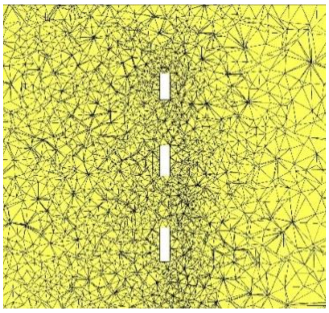

(c) Grid 1: section elev. a through slats (multi-level barriers)

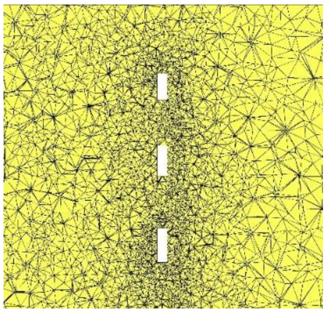

(d) Grid 2: section elev. a through slats (multi-level barriers)

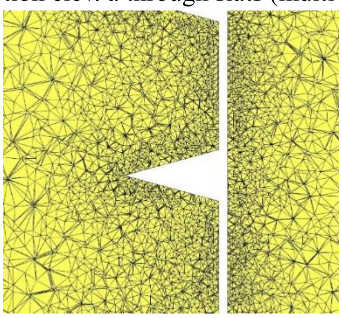

(e) Grid 1 : section plan B

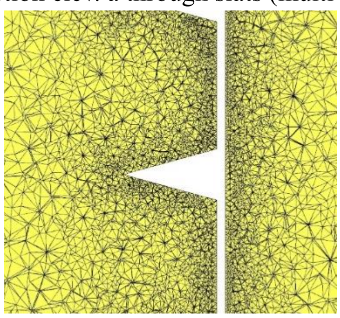

(f) Grid 2 : section plan B

Fig. 5 Details of utilized grids

Table 3 Grid, time based parameters

	G1	G2
Min Size (m)	0.00625	0.005
Growth Rate	1.2	1.2
Max Size (m)	0.05	0.05
Avg. Cell Count (x 10^6)	3	4.3
Time step (sec)	0.0004	0.00035
Simulation Time (sec)	10	10
Computation time (Hours)	16	27

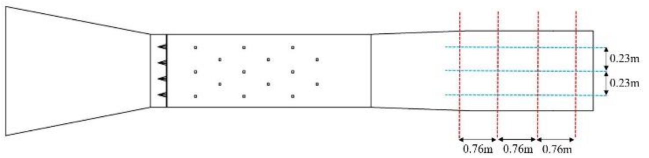

(a) Plan view of computational domain with 12 velocity acquisition locations

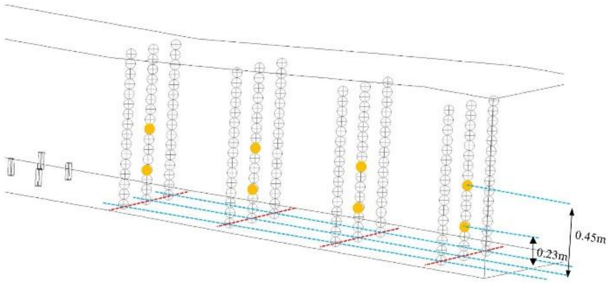

(b)Isometric view looking from above of the acquisition points

Fig. 6 Locations of velocity records

rows) as marked by the red lines and 3 across wind intervals (i.e., rows) as marked by the blue lines in Fig. 6(a). This 4 x 3 configuration resulted in a total of 12 locations where the (u) velocities were acquired. At each location, velocities at 16 intervals spaced every ~ .56 cm vertically, were extracted as shown in Fig. 6(b).

The study was conducted for 12 seconds of simulation time and data for first 2 second were truncated (i.e., 10 seconds were kept) to allow for the flow stabilization. Fig. 7 shows sample velocity-time history plot taken at rows 1-4 at column number 2 (i.e., centerline of the tunnel) at elevations z=0.23 m and 0.45 m (highlighted in orange in Fig. 6(b). The figure indicates that velocities fluctuate within a same range (i.e., ~15-30 m/s) between rows 3 and 4.

Figs. 8(a) - 8(c) show contour plots of the instantaneous velocities at a vertical section plane at the center of the tunnel, horizontal section plane at the mid-height of the tunnel and a horizontal plane passing through the roughness blocks, respectively. The three figures show how the turbulence generating elements abrupt the flow after the contraction zone until the turbulent flow averages out and gets uniform at the downstream zone of the diffuser. That is the zone where flow stabilizes and flow becomes suitable for building models.

The mean and root mean square (rms) of the velocities (after removing the first 2 seconds required for flow stabilization) were calculated and utilized to assess the adequacy of the resulting BL. Fig. 9 shows the mean and

Table 4 Summary of the first trial arrangement

Case Id	Elements No.	# of Columns	Height of blocks (cm)	Comments on Turbulence level
15RU5	15	5	5	Excessive turbulence at low heights
15RU10*	15	5	10	Acceptable up to 50 Cm
15RU15	15	5	15	Undesired Canopy layer
15RU20	15	5	20	Undesired canopy layer

Table 5 Summary of the staggered blocks results

Case Id	Element No.	Height of blocks	Staggered	Comments
4RS10	10 divided over 4 columns	10 cm	Yes	Profiles are closer to uniform than to BL
8RS10*	20 divided over 8 columns	10 cm	Yes	Results were close to the target ABL but not covered only 50 % of the tunnel
16RS10	40 divided over 16 columns	10 cm	Yes	Excessive turbulence was generated and could not cover the entire tunnel height

turbulence intensity profiles resulting from grids 1, 2 taken at the downstream (column 2 and row 4 in Fig. 6). As shown from the figure, the 2 grids led to almost identical profiles for both mean and turbulence intensity. The average discrepancy was in the order of 1.0 % for the mean velocity and 1.9% for the turbulence intensity, which deems adequate for grid independency of the results.

It is worth to mention that properties of Grid 1 were utilized for rest of the simulations. In the following section, simulations are conducted to assess the effect of various turbulence generating elements on the resulting BLs.

3. Effect of turbulence generating elements on the resulting BLS

This section shows Phase I of the study in which the behavior of BLs resulting from altering the turbulence generating elements including roughness blocks, spires, and barriers was investigated. This is to propose the most potential configuration (combination for the three elements) capable of generating target BL profiles. The effect of the roughness elements, spire height and utilization of slats (multi-level barriers) are investigated.

3.1 Effect of the roughness block elements

Effect of the roughness elements was assessed by varying the block height as summarized in Table 4. As indicated from Fig. 11, none of the resulting BLs matches the target. It was found out that the case of 10 cm roughness

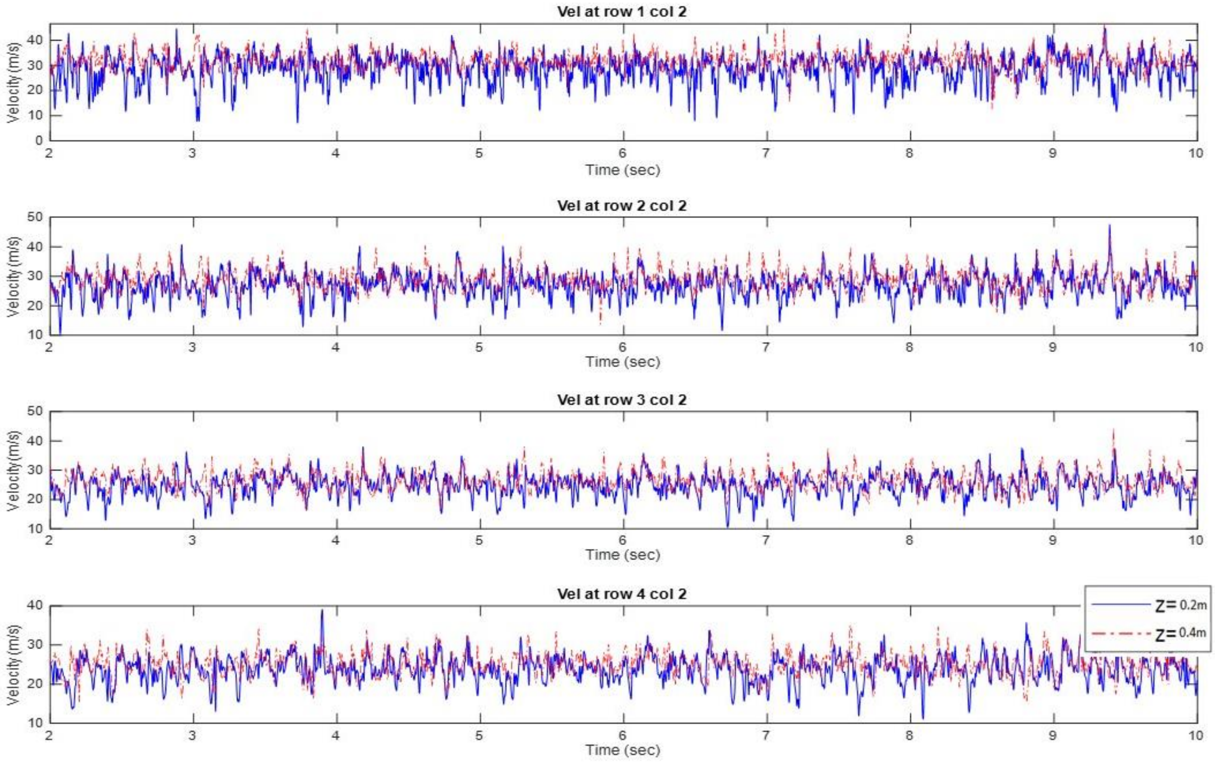

Fig. 7 Velocity-time history plot for row 1-4 at column number 2

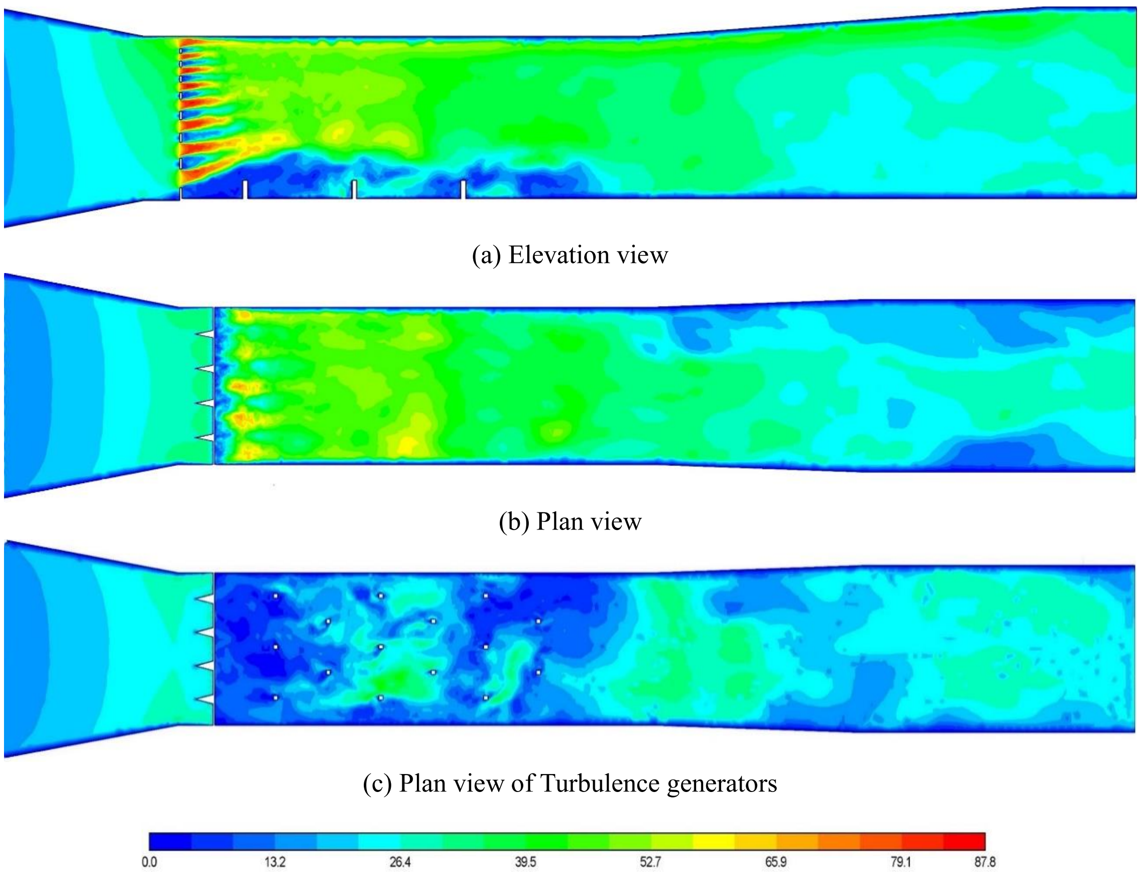

(a) Elevation view

(b) Plan view

(c) Plan view of Turbulence generators

Fig. 8 Contours of Instantaneous velocities (m/s)

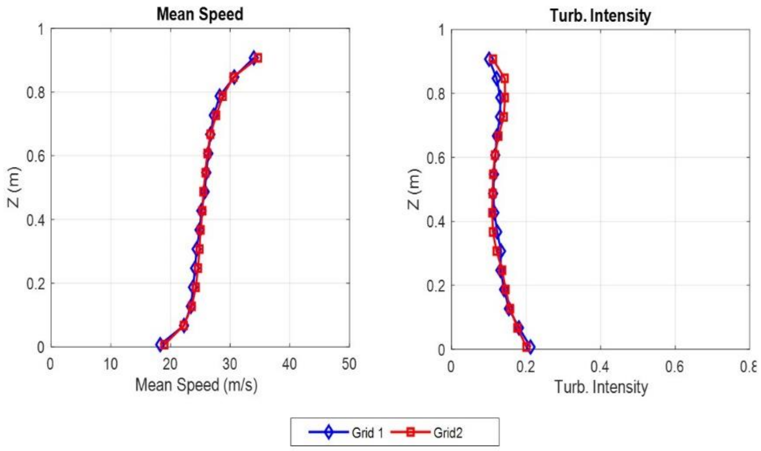

Fig. 9 Comparison between grid 1 and 2 mean and turbulence intensities

Table 4 Summary of the first trial arrangement

Case Id	Elements No.	# of Columns	Height of blocks (cm)	Comments on Turbulence level
15RU5	15	5	5	Excessive turbulence at low heights
15RU10*	15	5	10	Acceptable up to 50 Cm
15RU15	15	5	15	Undesired Canopy layer
15RU20	15	5	20	Undesired canopy layer

* Chosen as the most potential roughness height candidate for BL generation

Table 5 Summary of the staggered blocks results

Case Id	Element No.	Height of blocks	Staggered	Comments
4RS10	10 divided over 4 columns	10 cm	Yes	Profiles are closer to uniform than to BL
8RS10*	20 divided over 8 columns	10 cm	Yes	Results were close to the target ABL but not covered only 50 % of the tunnel
16RS10	40 divided over 16 columns	10 cm	Yes	Excessive Turbulence was generated and could not cover the entire tunnel height

* Chosen as the most potential roughness height candidate for BL generation

block led to a compatible boundary layer with the target however that was limited to heights up to the mid-tunnel height (i.e., 50 cm). Therefore, it was decided to utilize roughness block of 10 cm. Effect of block arrangement was investigated utilizing a constant block height of 10 cm as summarized in Table 5. Three arrangements were chosen as shown in Figure 12 and the results are shown in Fig. 13.

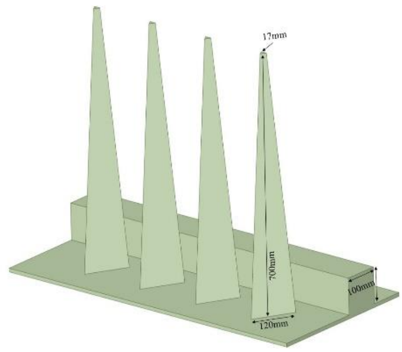

Fig. 10 Spire and barrier typical details

As shown in the tables, a case ID is given to each case, where the first two numbers refer to the number of blocks, third character "R" refers to roughness blocks, fourth character refers to U for uniform or S for staggered arrangements, and the last 2 numbers refer to the block height. For example, 15RU10 represents 15 uniform blocks with 10 cm height.

As summarized in Table 4, four different roughness heights varying between 5.0-20.0 cm were utilized, where the spire and the barrier are kept the same. Figure 10 shows details of the utilized spire and barrier, where 4 spires were implemented with a triangular shape with width of 12 cm at bottom and 1.7 cm at the top extended to an overall height of 70 cm and a barrier of 10 cm height and 10 cm depth where used. This spire block system was chosen arbitrary and will be tuned later in the subsections 3.2 and 3.3.

Fig. 11 shows the effect of changing the roughness height on the resulting BL. The figure shows the mean velocity and turbulence intensity profiles resulting from the 4 roughness heights compared with typical BL profiles (i.e. open, suburban and urban), which where extracted from the (ESDU 2010). It is worth mentioning that ESDU profiles are scaled down using a 1:500 to compare with the CFD-profiles of the WT. This 1:500 scale is the typical scale used for tall buildings (BLWT, 2007).

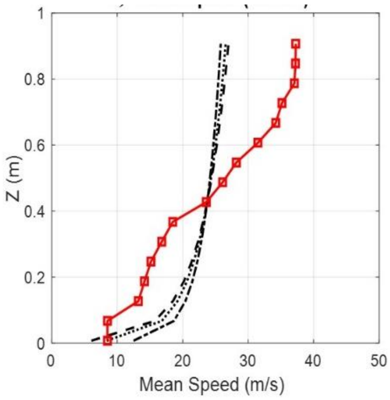

(a) Mean speed (15RU5)

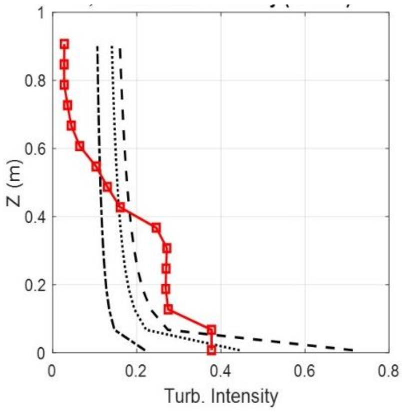

(b) Turbulence intensity (15RU5)

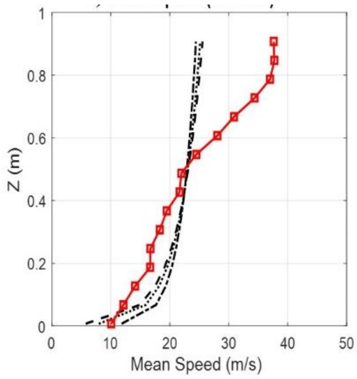

(c) Mean speed (15RU10)

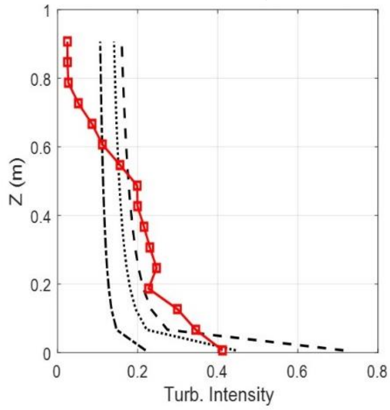

(d) Turbulence intensity (15RU10)

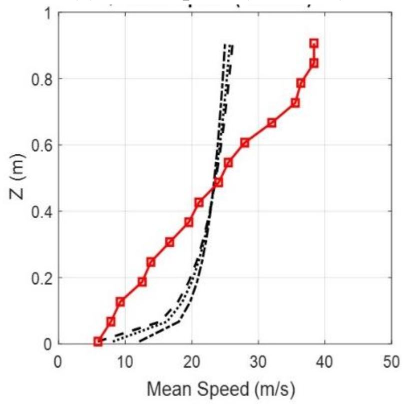

(e) Mean speed (15RU15)

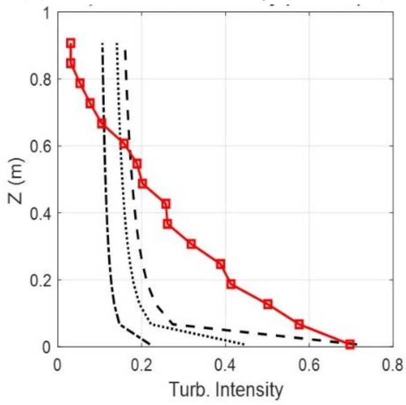

(f) Turbulence intensity (15RU15)

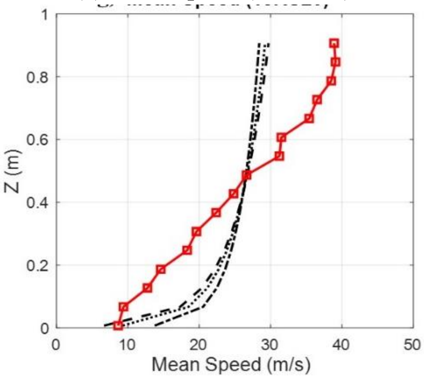

(g) Mean speed (15RU20)

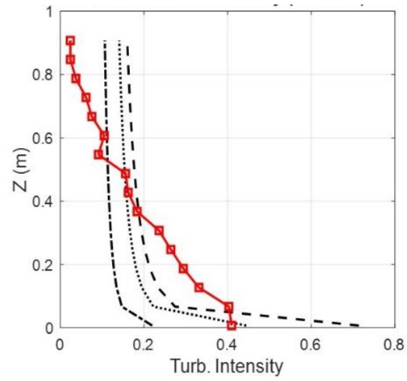

(h) Turbulence intensity (15RU20)

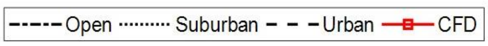

Fig. 11 Mean velocity and turbulence intensity for various blocks heights

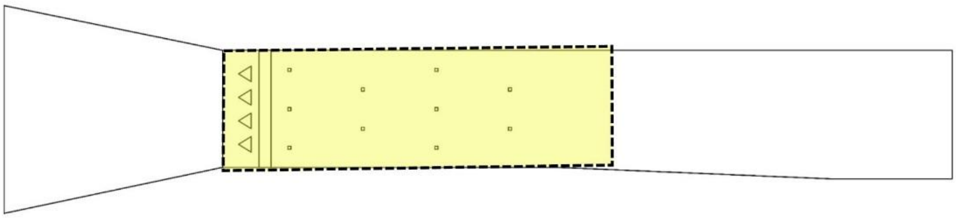

(a) 4 columns Staggered

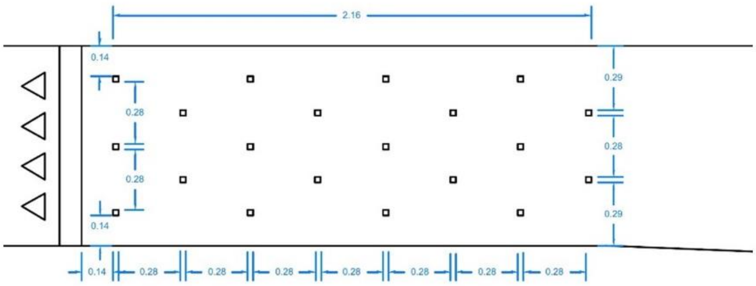

(b) 8 columns staggered

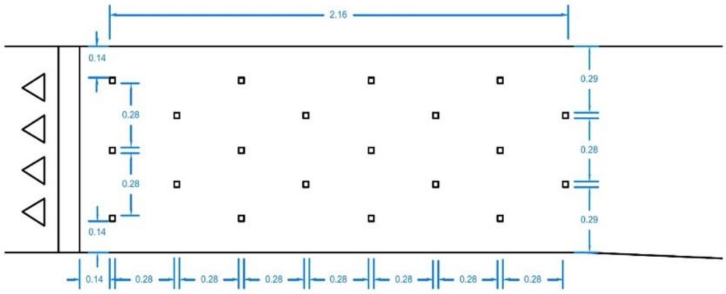

(c) 16 Columns Staggered

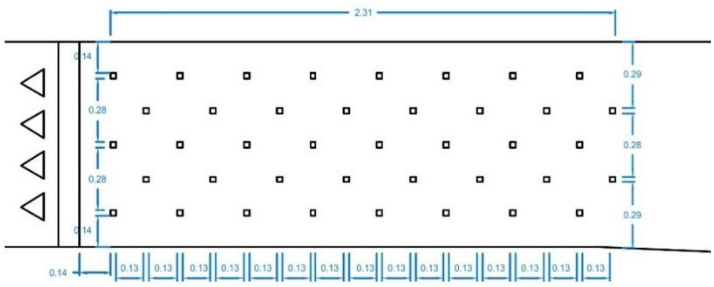

Fig. 12 Roughness block arrangement configuration (Dimensions in meters)

As indicated from Fig. 11, none of the resulting BLs matches the target. It was found out that the case of 10 cm roughness block led to a compatible boundary layer with the target however that was limited to heights up to the mid-tunnel height (i.e., 50 cm). Therefore, it was decided to utilize roughness block of 10 cm. Effect of block arrangement was investigated utilizing a constant block height of 10 cm as summarized in Table 5. Three arrangements were chosen as shown in Fig. 12 and the results are shown in Fig. 13.

It was found out by investigating Fig. 13 that only the case of 8RS10* with 8 staggered rows of 10 cm blocks led to acceptable results in terms of the turbulence intensity and mean velocity profile compared to those of the open terrain. However, that was true only up to the mid-height of the tunnel (i.e., 50 cm). Other staggering configurations, (i.e., 4RS10 or 16RS20), generates excessive turbulence close to the ground.
Since the case of 8 staggered 10 cm roughness blocks 8RS10 has shown the best match with the target profiles, it

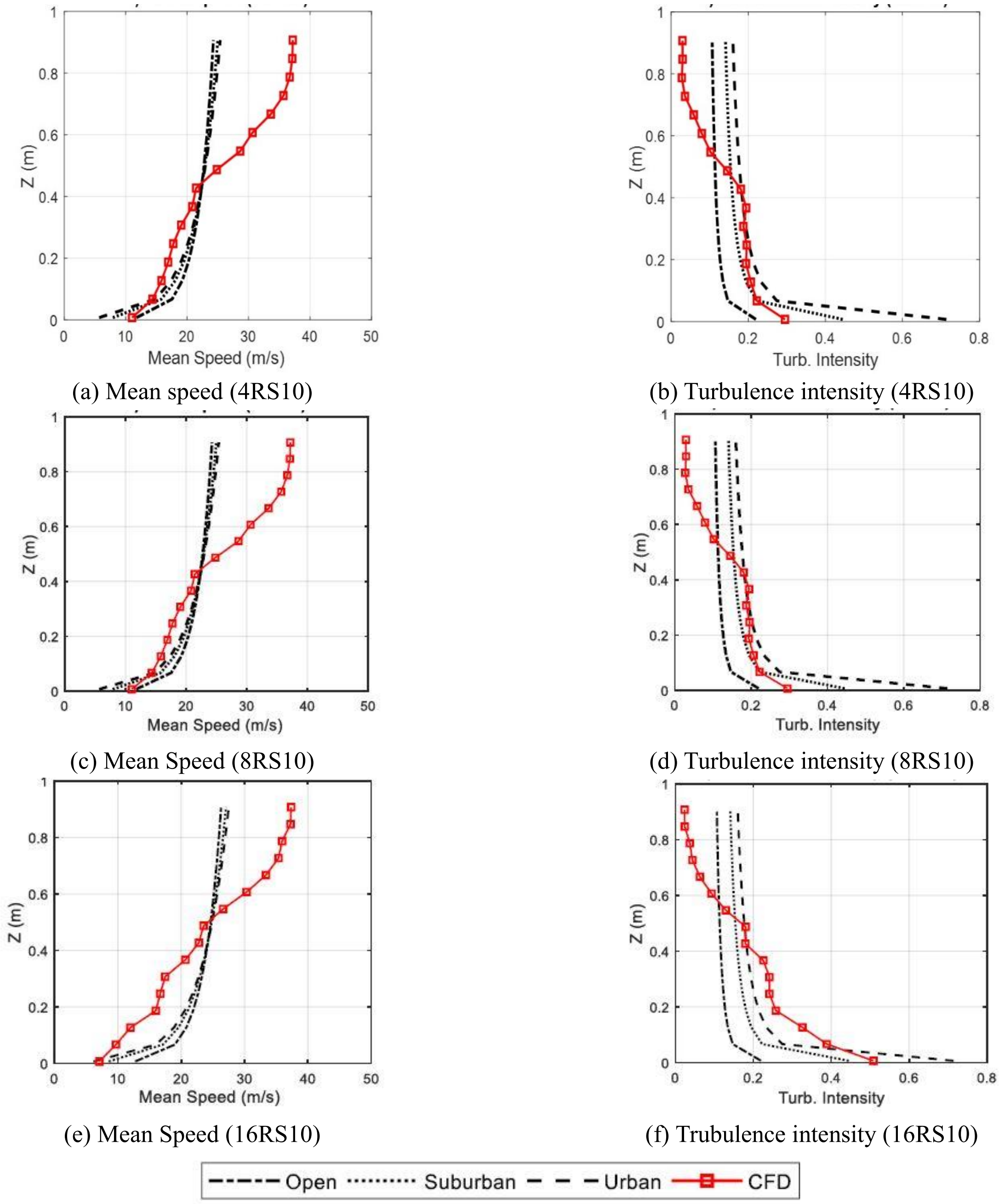

(a) Mean speed (4RS10)

(b) Turbulence intensity (4RS10)

(c) Mean Speed (8RS10)

(d) Turbulence intensity (8RS10)

(e) Mean Speed (16RS10)

(f) Trubulence intensity (16RS10)

Fig. 13 Mean velocity and turbulence intensity for staggered blocks arrangement

was decided to adopt it in the rest of the simulations, but with altering the spires with the aim to extend goodness of the match along the entire height of the tunnel.

3.2 Effect of the spire height

The case of 8 staggered 10 cm roughness blocks 8RS10 was adopted but with different spire heights. Spires similar to that shown in Fig. 10 were utilized but with a height of 50, 70 and 90 cm. All other spire dimensions were kept as in Fig. 10. Fig. 14 shows the profiles resulting from the 3 spire heights.

It was found out that, none of the spire lengths was able to generate proper turbulence intensity that covers the entire height of the tunnel. That is most-likely because of the limitation in the space available to condition the flow which is not long enough. For example, the distance from the contraction to the location where the flow is characterized is about 5.0m and the height of the tunnel is ~1.0 m. This will lead to a tunnel length-to-height ratio of 5.0/1.07=~ 4.6. When this ratio is compared with other tunnels, such as BL WT II as UWO, with a length of 40 m and a height of 2.5 m, the ratio is about 15, which is 3 times larger. In order to overcome this challenge, additional turbulence generating element is needed with truncated spires, as inspired by Kozmar (2011) and Varshney (2012). It was decided to add multi-level horizontal barriers (i.e., referred to as slats) attached to a truncated system of slats (covering the entire

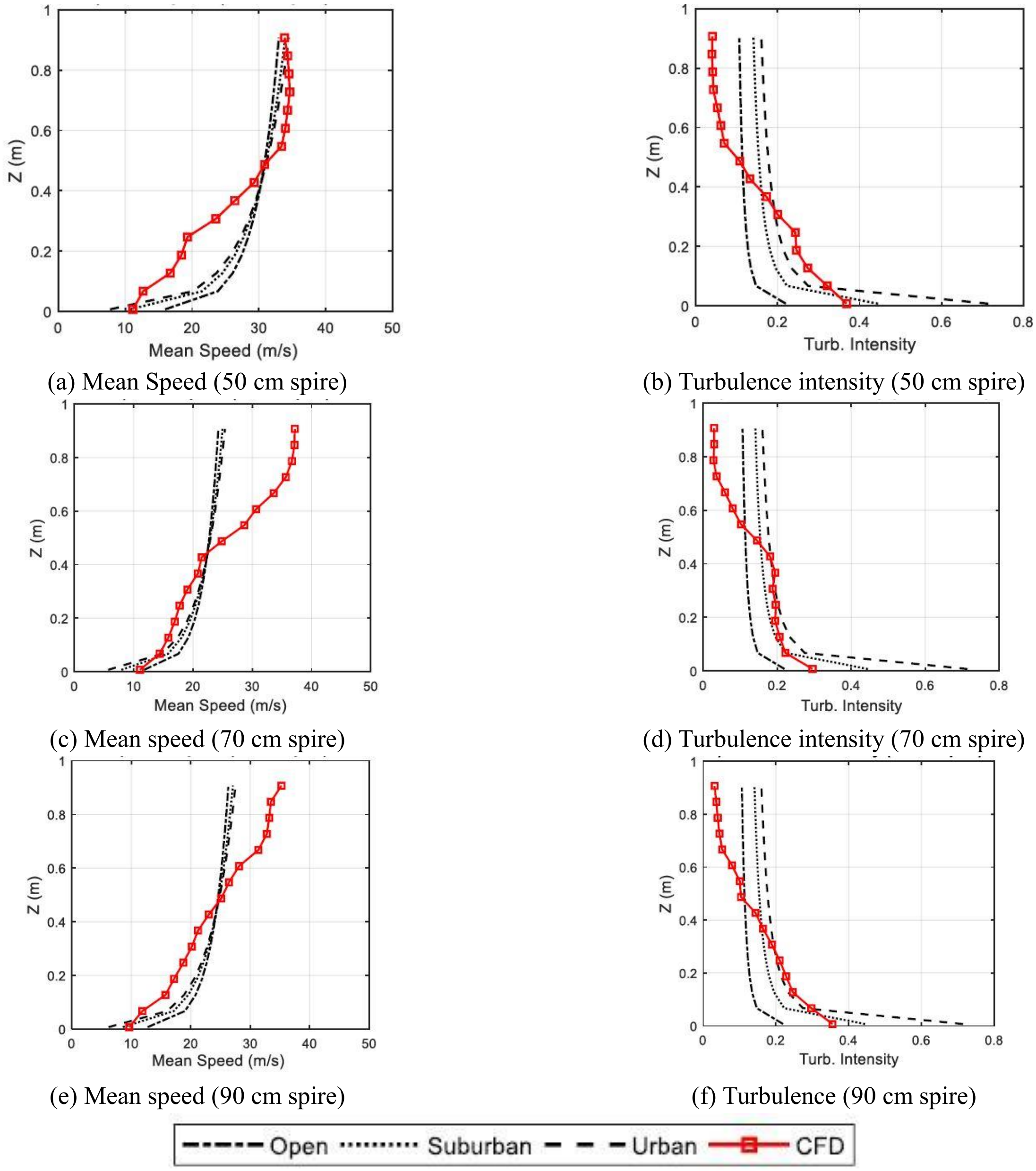

(a) Mean Speed (50 cm spire)
(b) Turbulence intensity (50 cm spire)
(c) Mean speed (70 cm spire)
(d) Turbulence intensity (70 cm spire)
(e) Mean speed (90 cm spire)
(f) Turbulence (90 cm spire)

Fig. 14 Mean wind speed and turbulence intensity for various spires heights

tunnel height of ~90 cm after the contraction) to introduce turbulence at the upper levels.

By investigating the current 90 cm high spires in Figure 14, it is clear that 90 cm spires lead to excessive turbulence intensity at the lower portion of the tunnel, which is unacceptable. Therefore, it was decided to change the bluff-body spires in Fig. 14 to a more streamlined ones as shown in Figure 16 to generate lesser turbulence. The slats were chosen to cover approximately 40% of the tunnel cross section. This 40% with the new stream-lined spires leads to approximately same total drag force as that from the original spires with a 10 cm barrier. Effect of the slat distribution is investigated in the following subsection.

3.3 Effect of slat arrangement (i.e., horizontal barriers)

Simulations were conducted for the system with 2 slat arrangements shown in Fig. 16: (i) uniform slats, and (ii) tapering slats with a starting height of 9 cm at the base (~ 0.085 of the tunnel height downstream) and 2 cm at the top (~ 0.019 of the tunnel height downstream). A number of 8 slats were chosen for the two setups where the blockage was kept constant at 40% for the two cases to assess the effect of slat profile. Fig. 17 shows the mean velocity and turbulence intensity profiles for the two slat configurations compared with target ESDU profiles. It was found out that the case of tapered slats generated the results matching those of the open terrain exposure along the entire depth of the tunnel. Therefore, this configuration of tapering slats with 40% blockage is adopted in the flow conditioning

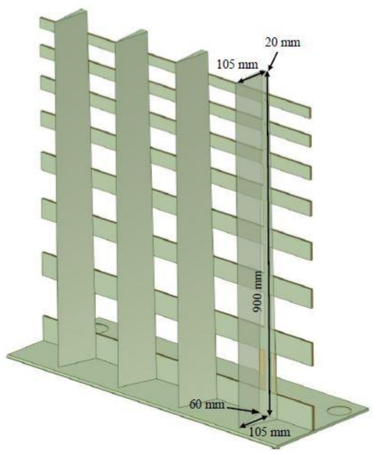

Fig. 15 Spire-Slat System

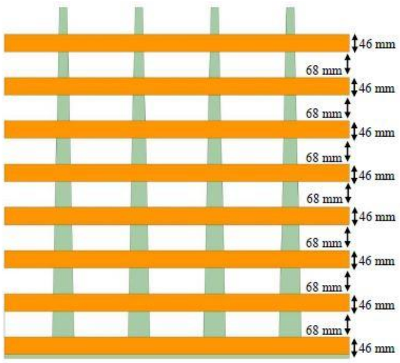

(a) Elevation view normal to the slats uniform slats covering 40%

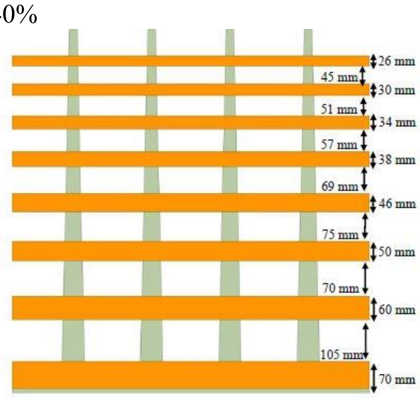

(b) Elevation view normal to the slats tapering slats covering 40%

Fig. 16 Slat arrangements

system design.

Since the 40% blockage generated a BL that matched the open terrain, it is expected that rougher (i.e. suburban or urban) terrains can be generated by increasing the blockage. This led to the suggested design of the slat-spire system shown in Fig. 18 where two-layer slats are employed: (i) a fixed upwind layer with a 40% blockage and (ii) movable downwind layer with also 40% blockage. This system allows for controlling the blockage between the range of 40-80%. When the two-layer system is fully open, as shown in, Fig. 18(a) the overall blockage is just 40% (i.e., second layer is completely shielded), but when the system is fully closed, as shown in Fig. 18(a) the overall blockage increases to 80%, where the second layer is fully exposed to wind. Fig. 18(b) shows an intermediate case, where the second layer is 50% shielded and the blockage is 60%.

Moreover, the power spectral density (PSD) was obtained for the longitudinal velocity (at the mid-height of the tunnel) and generated from the fully open system (i.e. 40% blockage) as shown Fig. 19. The resulting PSD was compared with the target von Karman Spectra (ESDU, 1974-1975) evaluated using Eq. (2). It was found out that PSD of the fully opened system perfectly matches the spectra of the open terrain at different frequencies. This proves adequacy of the system to simulate proper open terrain BL when at 40% blockage.

$$S_u = \frac{4x}{(1+70.8x^2)^{5/6}}, x = \frac{fL_u}{V}, L_u = 25z^{0.35}z_0^{-0.063} \tag{2}$$

where f is the frequency, V is the mean wind speed, L_u is the longitudinal turbulence length scale, z is the height from the ground, z_0 is the aerodynamic roughness taken as 0.03 m,0.3 m and 0.7 m for open, suburban and urban terrain exposures, respectively.

It is worth mentioning in the PSD plots that, a cut off frequency was highlighted on the plot, which represents the maximum frequency that can be predicted from the CFD simulation (Aboshosha *et al*. 2015).

In the next section, alternation to the movable layer of slats is conducted to generate BLs matching suburban and urban terrains.

4. Tuning for suburban and urban BLS

The two-layer spire-slat system shown in Fig. 18 was utilized here to generate BLs matching suburban and urban terrains. Slats are grouped into 4 groups with 2 slats in each group. Each group can move at a different distance (or at a different rate) independently. This was achieved by connecting each group to a rotary shaft using links connected at different radii as shown in Fig. 20. The larger the radius of movement, the greater the distance the slat group travels. Since larger slats are located at the bottom, larger radii were used with lower slat groups.

A large number of LES were conducted to find the best slat combination representing the target profiles. Table 6 summarizes the slat movement required to achieve best BLs matching suburban and urban exposures. It was found out that the system with no slat movement leads to the best matching BL for open terrain as illustrated previously in Fig. 17(b) and Fig. 19. Fig. 21 shows the results for the suburban profile, while Fig. 22 shows the results for the urban profile. As it can be seen, the recommended slat combinations led to a very good match. It was found out that the average discrepancy in the mean velocity profile from the system and the target is about 2.0% for the open terrain, and 2.5% for the suburban terrain. With respect to the suburban terrain, the discrepancy was found to be 3.2% and 3.6% for the open and suburban terrain, respectively. This proves that the suggested spire-slat system allows for modeling wide range of BLs (i.e., from open to

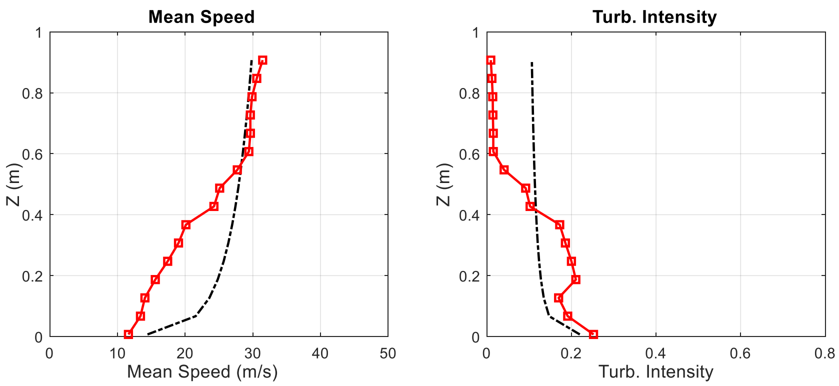

(a) Uniform slats

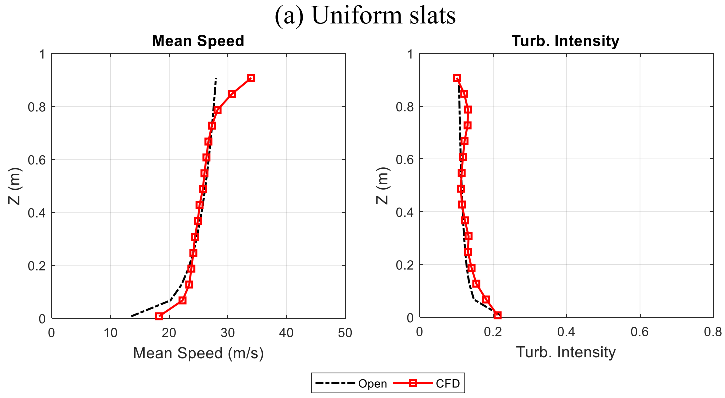

(b) Tapered slats

Fig. 17 Mean wind speed and turbulence intensity

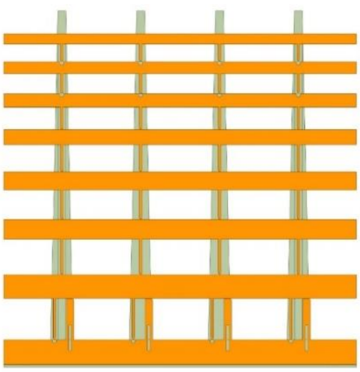

(a) fully open

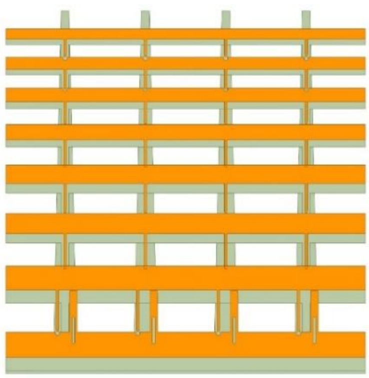

(b) partially open

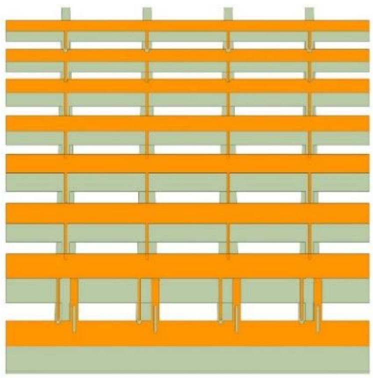

(c) fully closed

Fig. 18 (a) fully open, (b) partially open, (c) fully closed

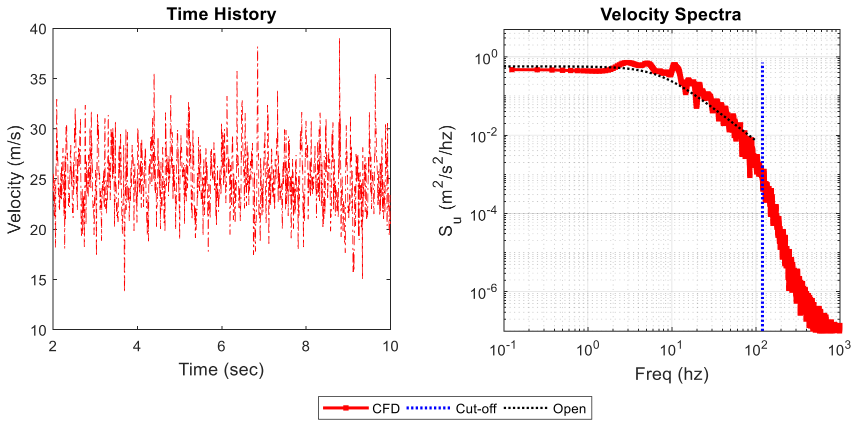

Fig. 19 Velocity-Time history for the fully opened system and PSD compared with ESDU

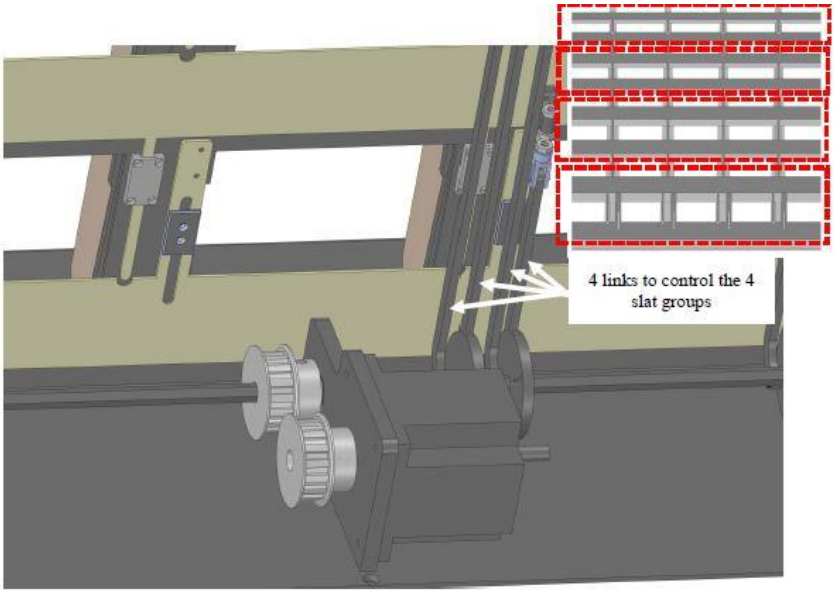

Fig. 20 Controlling slat groups at different rates

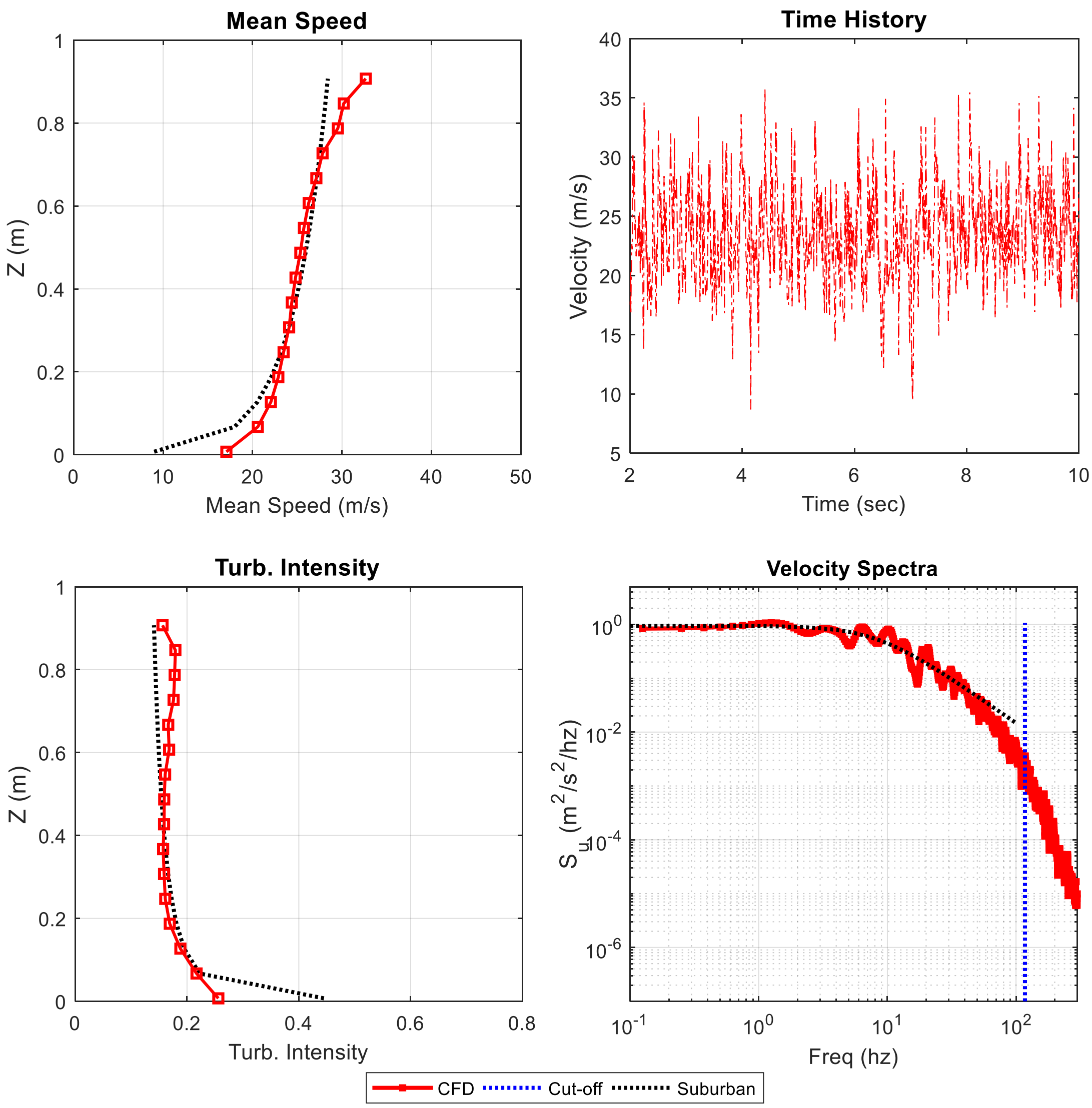

Fig. 21 Mean speed, Turbulence intensity and spectra for Suburban terrain

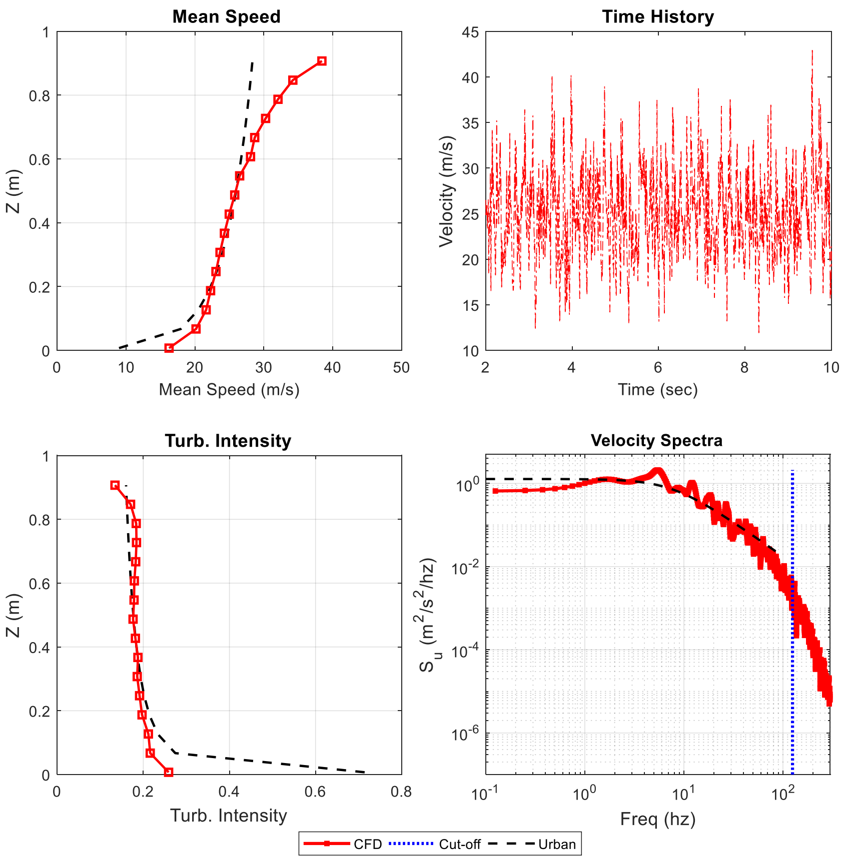

Fig. 22 Mean speed, Turbulence intensity and spectra for urban terrain

urban) and any combination in-between.

It is worth mentioning that CFD simulations have shown that the flow-conditioning system, consisting of: (i) two-layer spire-slat system, (ii) 10 cm roughness staggered roughness blocks distributed over 6 rows, can successfully generate a wide range of BLs. The system which is shown in Figure 23 was constructed and validated experimentally at RU WT as will be discussed in following section (Section 5).

5. Experimental validation

This section discusses the experimental validation of the flow conditioning system at RU wind tunnel and is divided into 3 subsections. First, Subsection 5.1 discusses the details of the experimental system as well as results regarding the flow quality (i.e., uniformity) at the chosen testing zone of the wind tunnel. This followed by Subsection 5.2, which presents the resulting BL flow field that match the target BLs at two different length scales typically used for tall buildings (i.e., 1:500 and 1:250).

5.1 Details of the experimental setup

The flow conditioning system was constructed and installed at RU wind tunnel as shown in Fig. 24. Fig. 24(a) shows component of the spire-slat system, while Figs. 24(b) and 24(c) show the system at the fully open and fully closed positions. This system is controlled using a stepper motor (NEMA 34), with a high torque of 1100 oz-in (7.8 N.m) capable of moving the slats smoothly at wind speeds up to 60 m/s.

Turbulent wind speed profiles in the tunnel were characterized using 2 multi-hole pressure probe (Cobra Probes) namely Probe A and Probe B as shown in Figure 25. In order to confirm repeatability of the results obtained from the tunnel, Probe A was always kept at a same location at the center of the turntable at 0.2 m high. Probe B was the movable probe and utilized to acquire the turbulent speeds at different heights and locations of the tunnel. Those probes have a sampling frequency of 1250 hz and are capable of capturing inclined turbulent speeds within ±45° from the main flow direction. The probes were utilized to characterize the turbulent speeds at 8 heights (0.1, 0.2, 0.3, 0.4, 0.5, 0.6, 0.7 and 0.8 m).

Table 6 Slat Group Movement with Respect to Open Terrain Slat Configuration

	Open Terrain	Suburban Terrain	Urban Terrain
Slat Groups		Slat Movement (mm)	
Group 1 (bottom)	0	8	13
Group 2	0	6	10
Group 3	0	2	4
Group 4 (top)	0	2	3

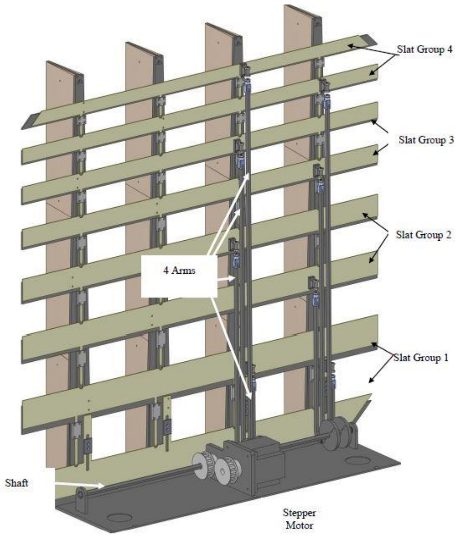

Fig. 23 Two layer spire-slat system

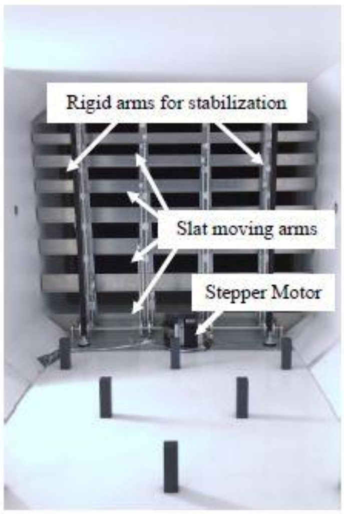

(a) Elevation view with stepper motor to control the slats opening

(b) Slats fully opened

(c) Slats fully closed

Fig. 24 Flow conditioning system a) Elevation view showing the stepper motor b) Slats fully opened (40% blockage) c) Slats fully closed (80% blockage)

Quality of the resulting flow at the turntable was investigated using Cobra Probes. This was conducted by acquiring the turbulent velocities at 4 locations shown in Fig. 26. The four locations are taken at (i) the middle of the tunnel at the center of the turntable and denoted by “M”, (ii) quarter of the turntable to the left and detonated by “L”,

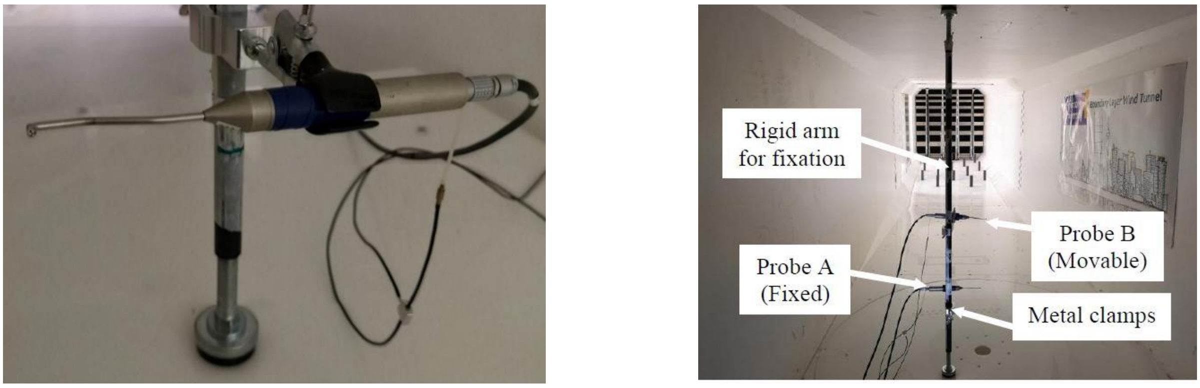

Fig. 25 Probes setup and fixation

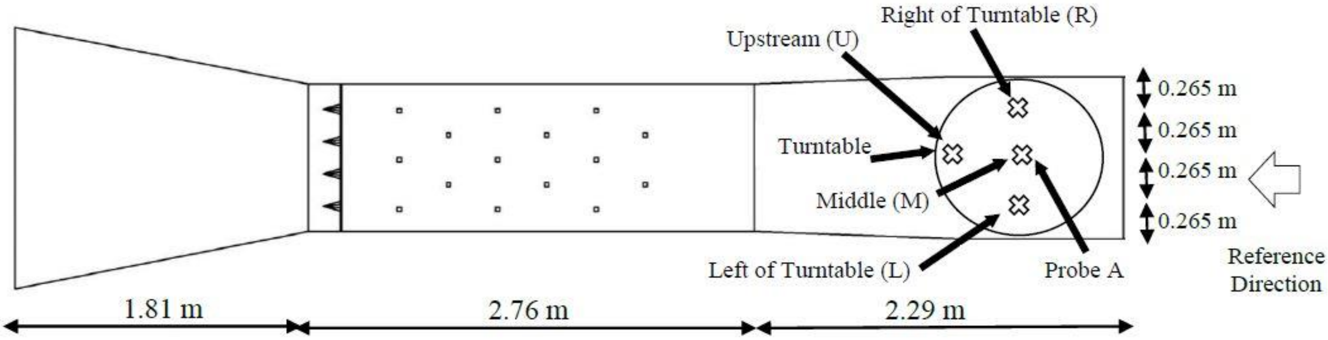

Fig. 26 Uniformity test location

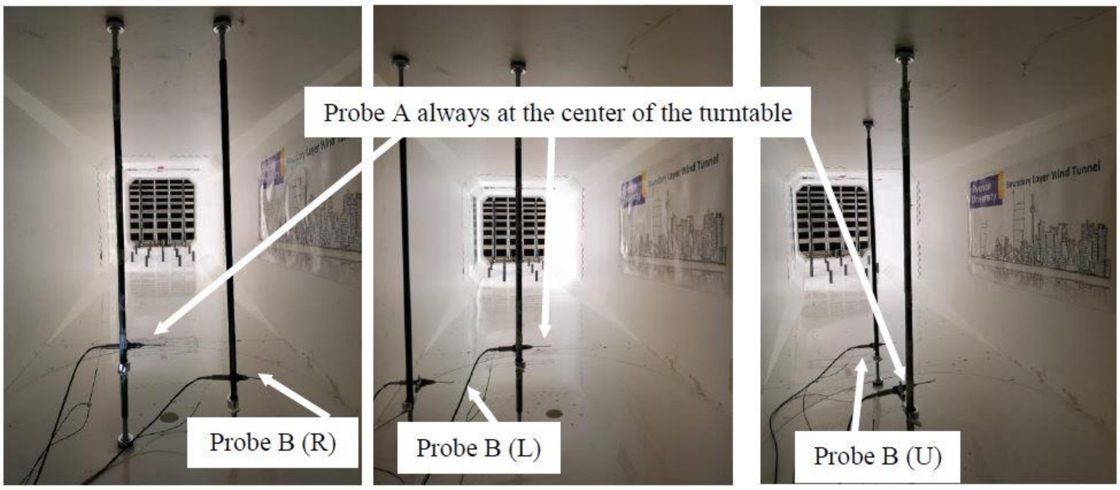

(a) Probe B on the right (b) Probe B on the left (c) Probe B on the left

Fig. 27 Uniformity test at different locations

(iii) quarter of the turntable and denoted by “R”, and (iv) upstream the turntable at the middle and denoted by “U”.Probe B was utilized to obtain wind velocity records at the four locations at various heights. Images showing sample probe layouts are provided in Fig. 27.

Mean longitudinal wind velocities and longitudinal turbulence intensities where evaluated for the fully open wind spire-slat system and plotted in Fig. 28 at the four selected locations. The figure indicates that the obtained four profiles are in a reasonable good agreement with each other and, therefore it can be concluded that uniformity of the obtained flow field is acceptable at the test zone (i.e. within the limits of the turntable).

5.2 Validating the resulting BL wind field

Turbulent velocity records in the longitudinal u, transverse v, and vertical w directions were acquired at the center of the turntable at various heights considering different Spire-slat openings. First, slat-openings as

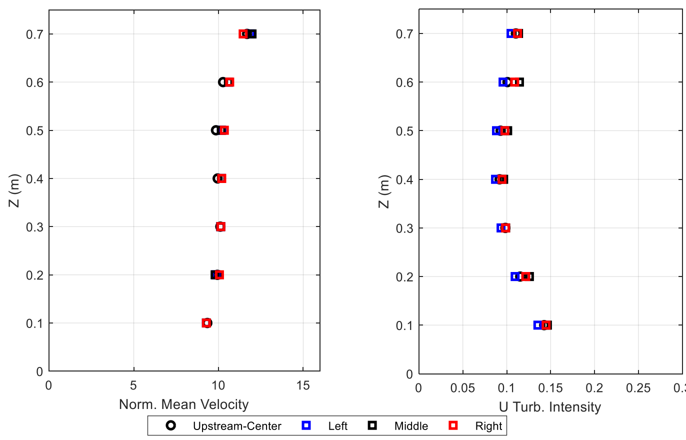

(a) Mean speed (b) Turbulence intensity (I_u)

Fig. 28 Mean speed and turbulence intensity at four locations in the turntable

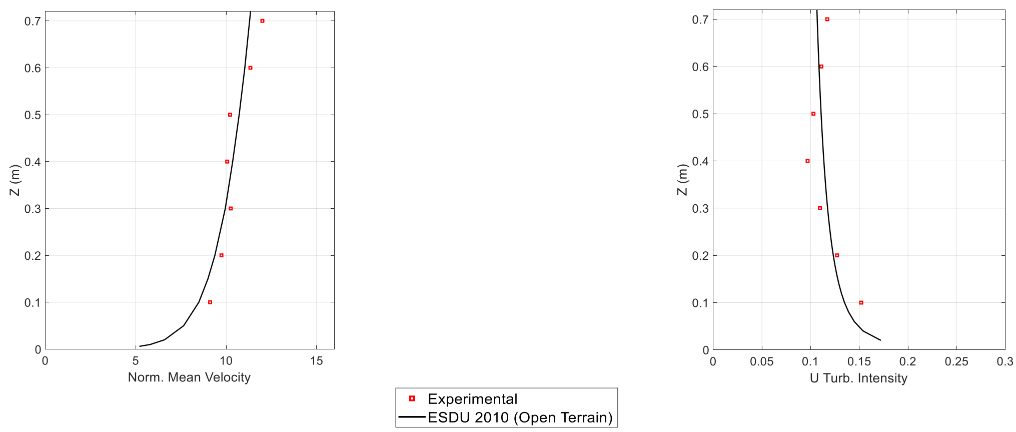

(a) Mean velocity (b) I_u Turbulence intensity

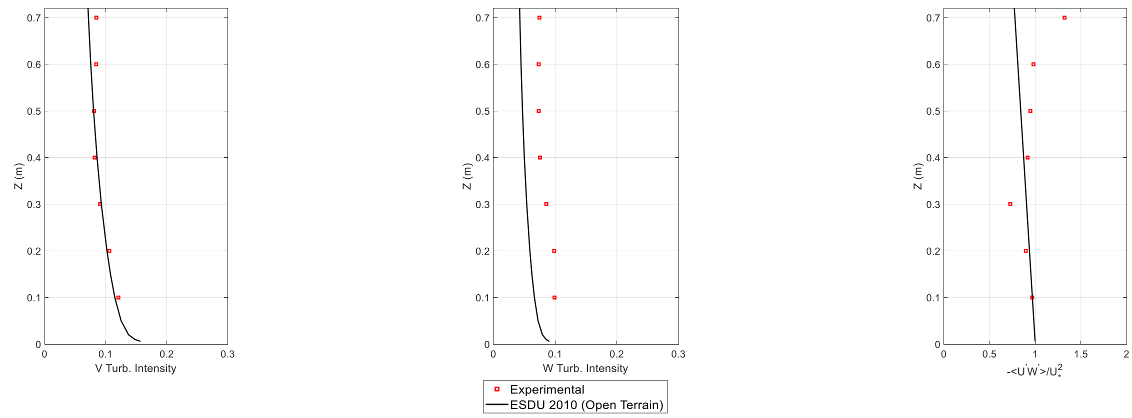

(c) I_v Turbulence intensity (d) I_w Turbulence intensity (e) <$u'w'$> Reynolds stress

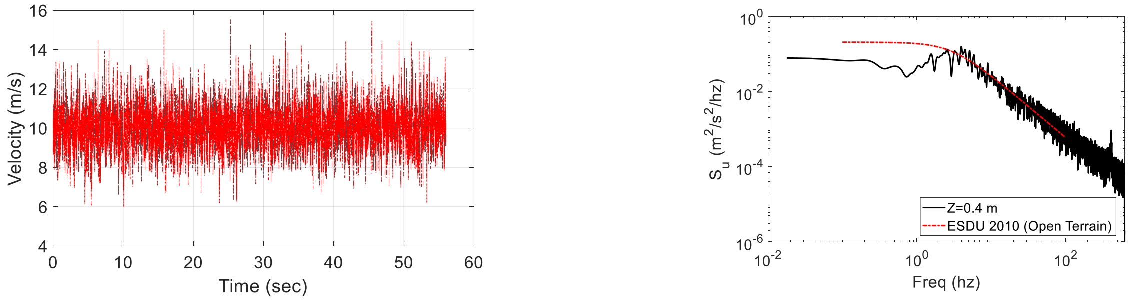

(f) Sample velocity time history at 0.4 m (g) PSD

Fig. 29 Wind field characteristics best matching open terrain exposure at L_{scale} of 1:500 (R=45%)

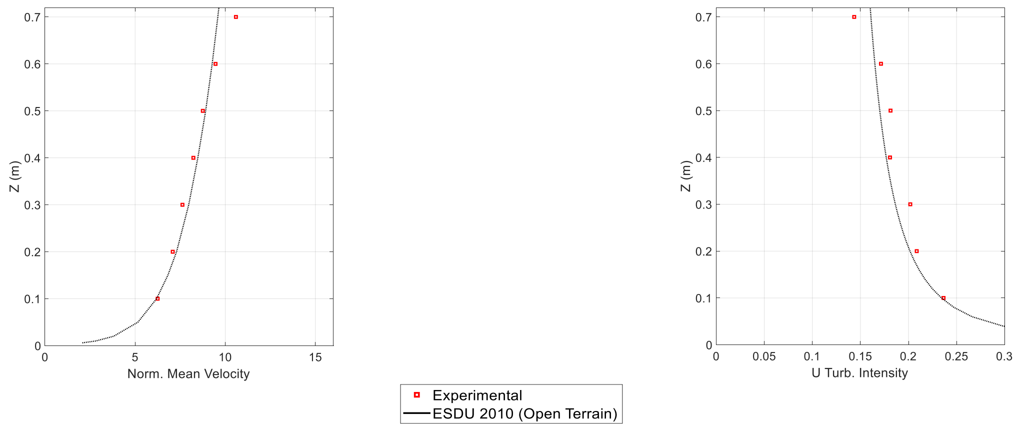

(a) Mean velocity (b) I_u Turbulence intensity

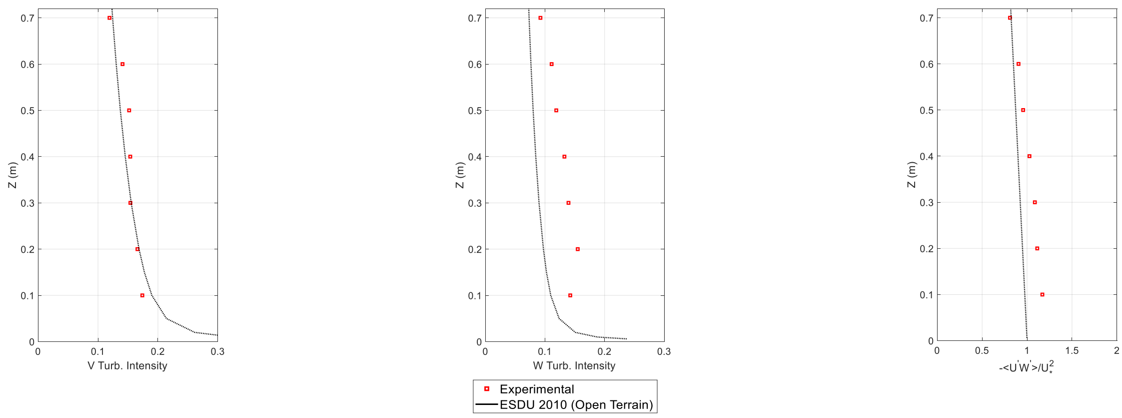

(c) I_v Turbulence intensity (d) I_w Turbulence intensity (e) $<u'w'>$ Reynolds stress

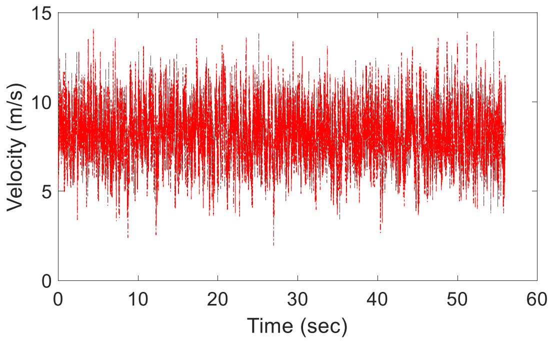

(f) Sample velocity time history at 0.4 m

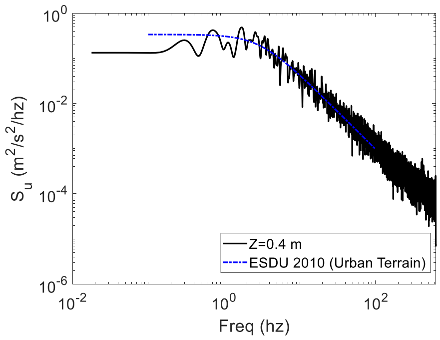

(g) PSD

Fig. 30 Wind field characteristics best matching suburban terrain exposure at L_{scale} of 1:500 (R=55%)

suggested from the CFD was used, and the profiles were compared with the target profiles according to the ESDU.

Then, the openings were slightly adjusted until the resulting profiles best match the target. Target profiles were taken considering two sample length scales typically used for tall buildings (i.e., 1:500 and 1:250). Fig. 29 shows the resulting profiles at the center of the turntable for an open terrain exposure for a length scale of 1:500. As shown in the figure, longitudinal mean velocity, turbulent intensities I_u, I_v and I_w and Reynolds stress $<u'w'>$ are plotted and compared with the target. In addition, sample longitudinal velocity time history at 0.4m is plotted and its spectra was generated and compared with target according to the ESDU (2010). It can be seen from Figure 29 that resulting flow field characteristics match those of the ESDU with a very good agreement. There is a slight overestimation of the I_w component, but this is expected to have a minor effect on the building pressures and associated later loads.

Similarly, Figs. 30 and 31 show the resulting wind field from the system at a length scale of 1:500 compared to the target suburban and urban ESDU profiles, respectively. The two figures show very good match which validates the designed system. Similar to Figs 29 - 31, Figs 32 - 34 present characteristics of the resulting flow field compared with the ESDU for open, suburban and urban terrain exposures, respectively, at a length scale of 1:250. Those figures also confirm the accuracy of the system in generating target BL winds. The effective blockage for each of the cases presented in Figures 29-34 is shown on the figure caption. It can be seen that, the required blockage to

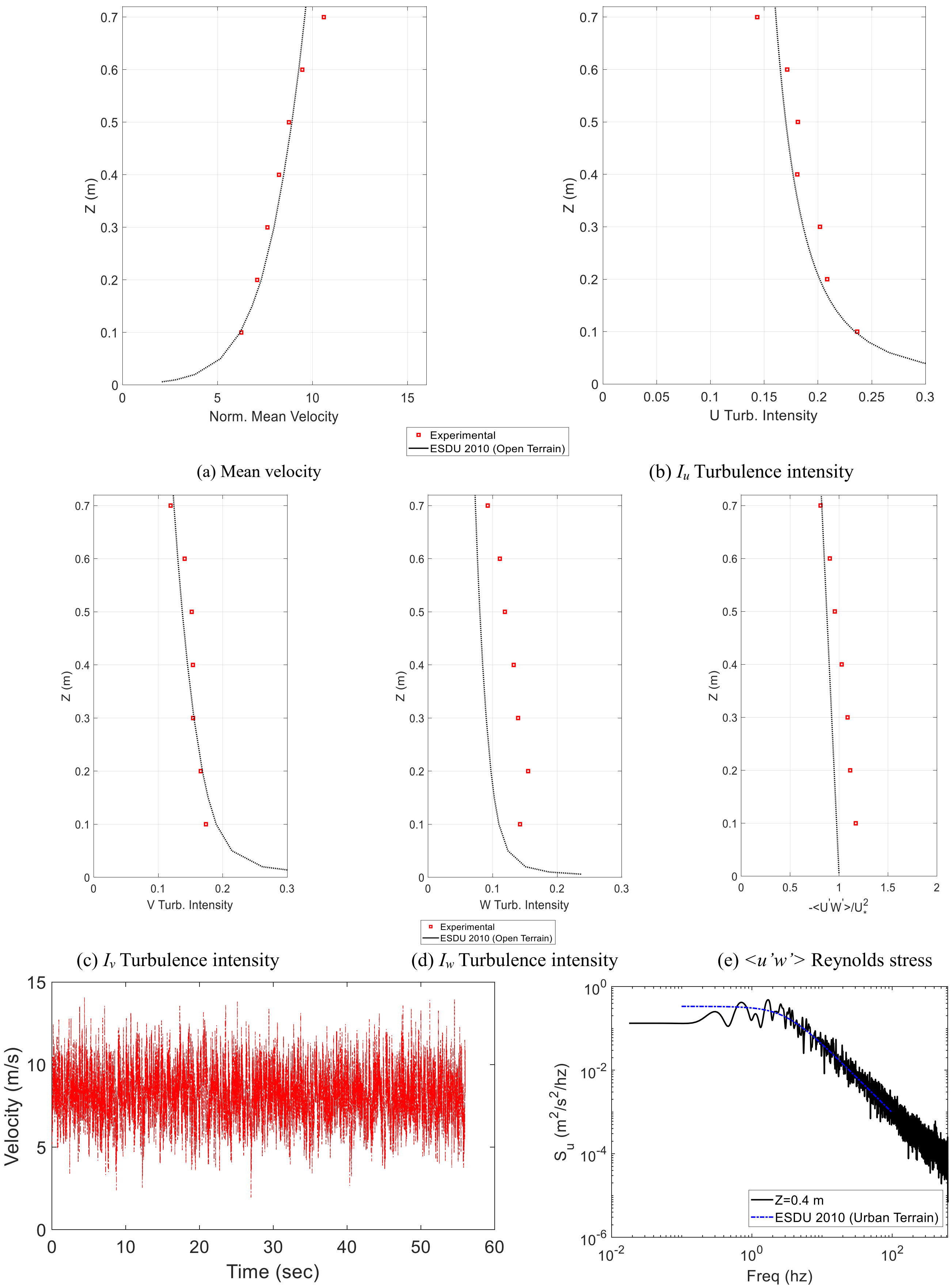

(a) Mean velocity

(b) I_u Turbulence intensity

(c) I_v Turbulence intensity

(d) I_w Turbulence intensity

(e) <*u'w'*> Reynolds stress

(f) Sample velocity time history at 0.4 m

(g) PSD

Fig. 31 Wind field characteristics best matching urban terrain exposure at L_{scale} of 1:500 (R=63%)

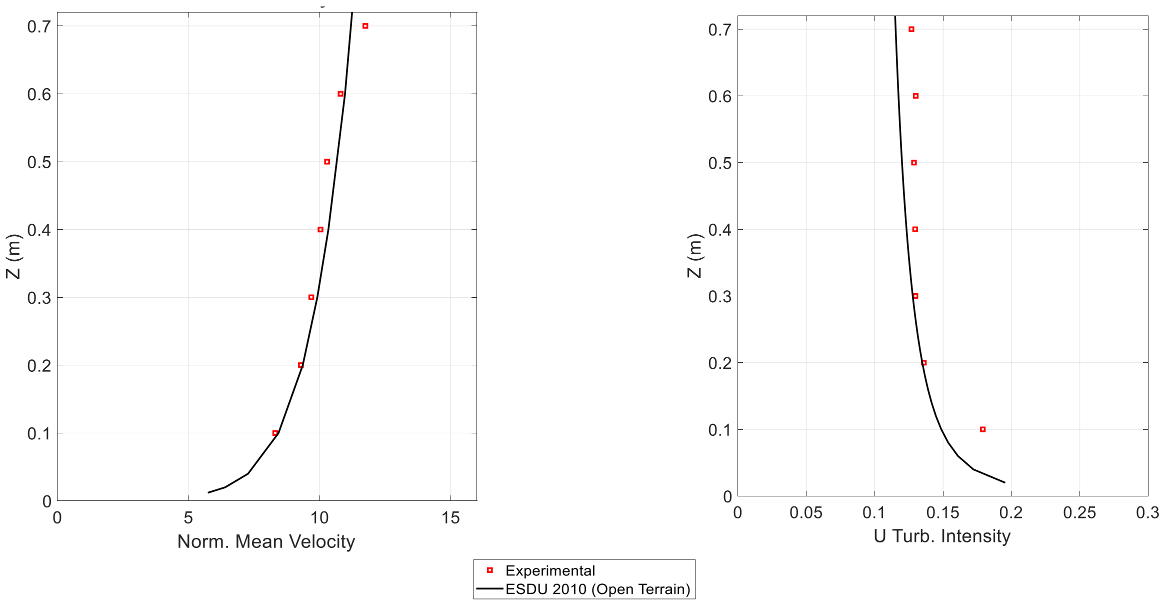

(a) Mean velocity (b) I_u Turbulence intensity

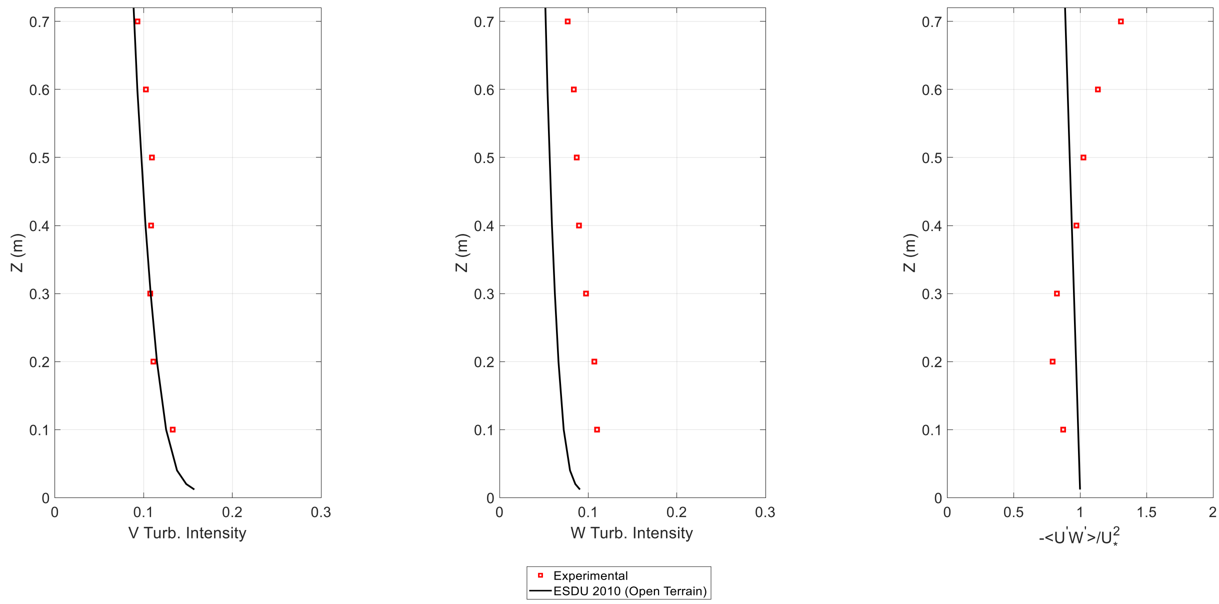

(c) I_v Turbulence intensity (d) I_w Turbulence intensity (e) <$u'w'$> Reynolds stress

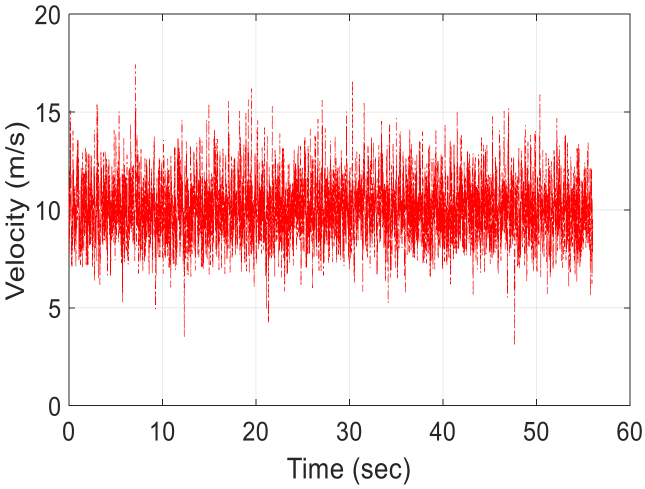

(f) Sample velocity time history at 0.4 m

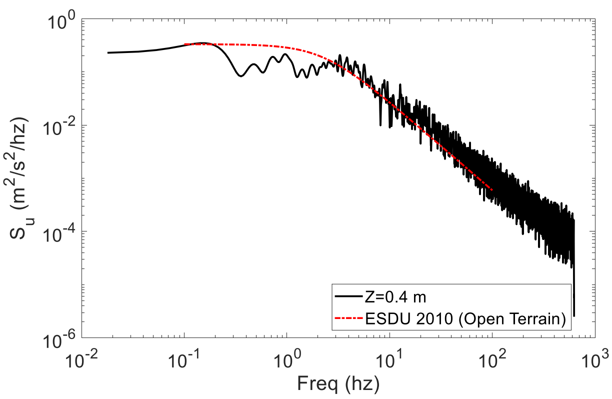

(g) PSD

Fig. 32 Wind field characteristics best matching open terrain exposure at L_{scale} of 1:250 (R=48%)

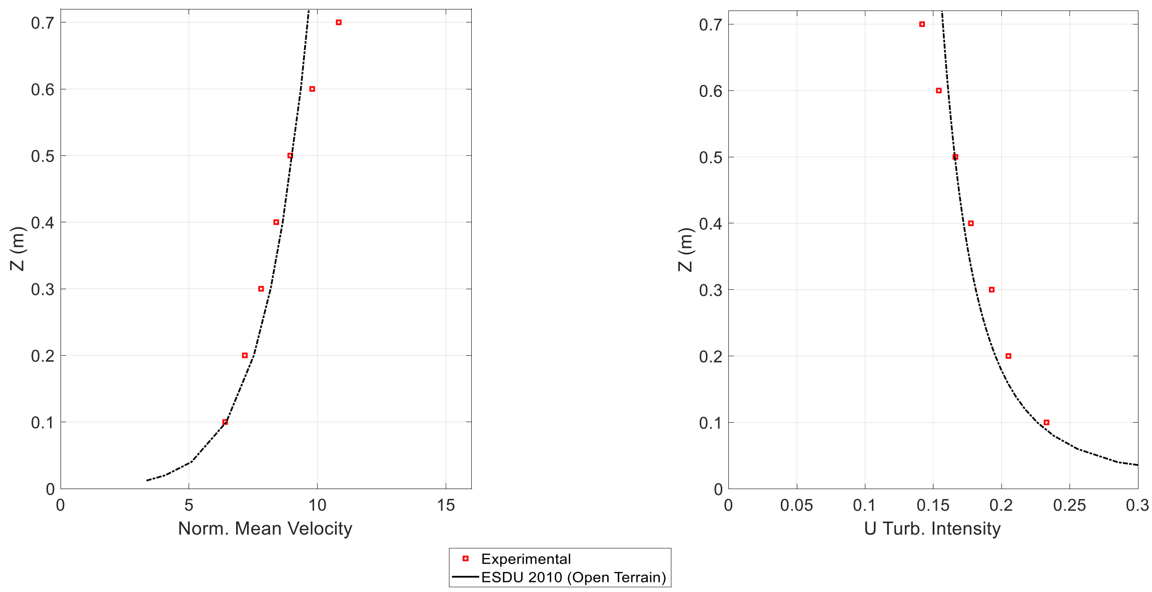

(a) Mean velocity (b) I_u Turbulence intensity

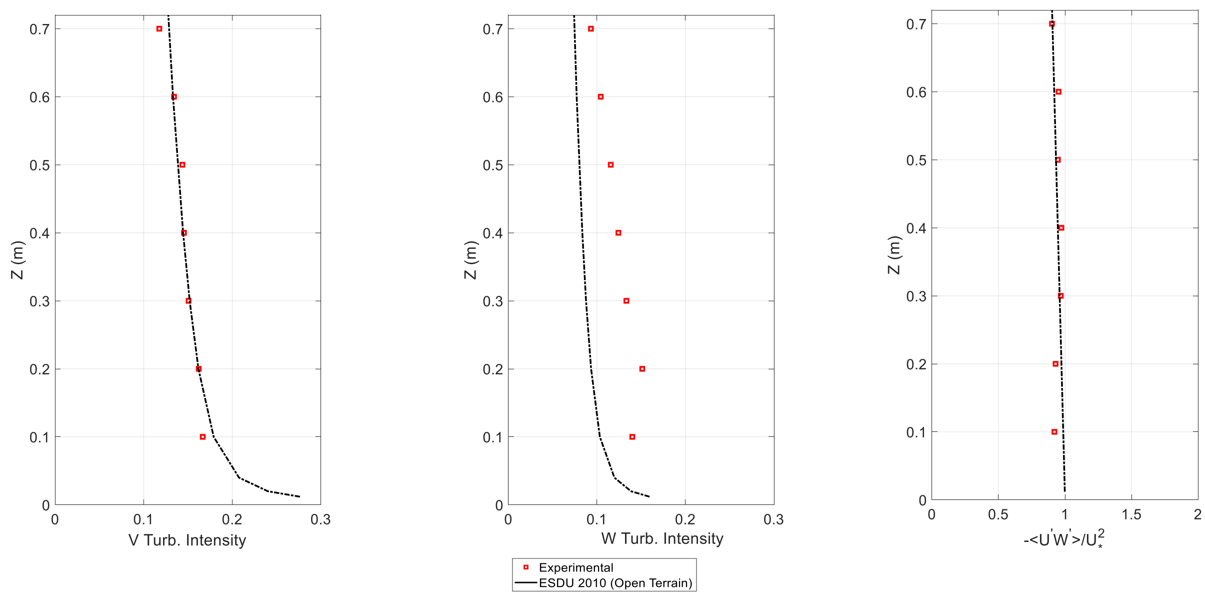

(c) I_v Turbulence intensity (d) I_w Turbulence intensity (e) $<u'w'>$ Reynolds stress

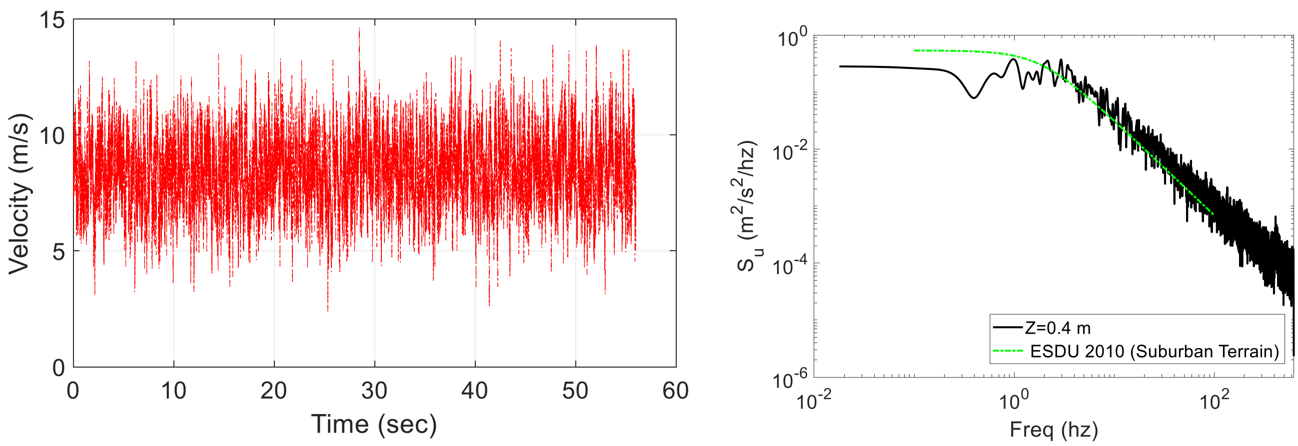

(f) Sample velocity time history at 0.4 m (g) PSD

Fig. 33 Wind field characteristics best matching suburban terrain exposure at L_{scale} of 1:250 (R=62%)

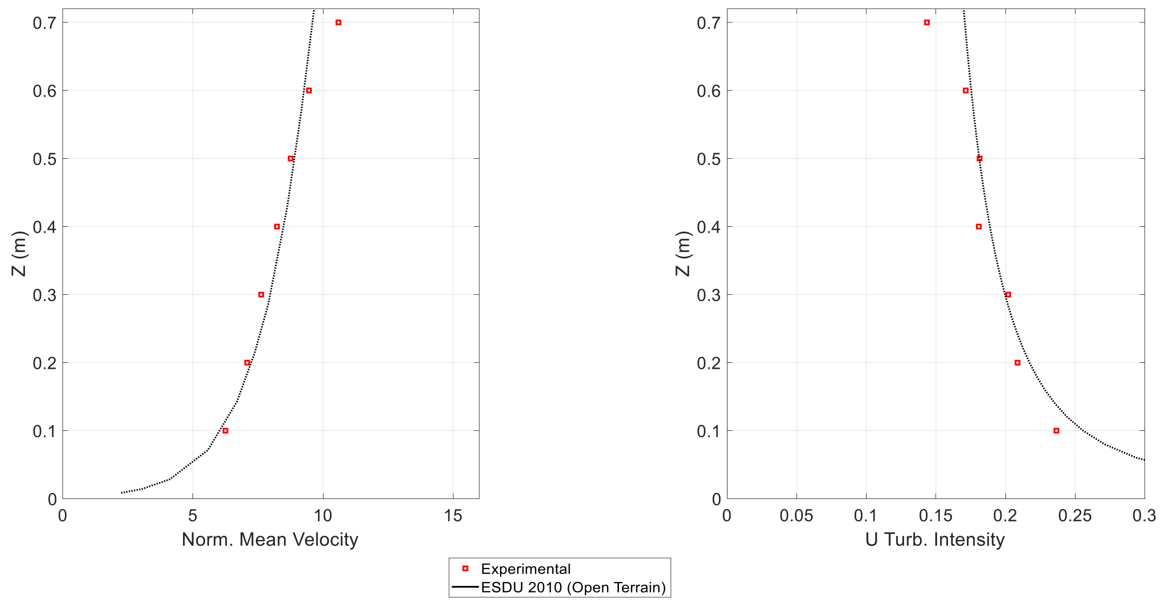

(a) Mean velocity (b) I_u Turbulence intensity

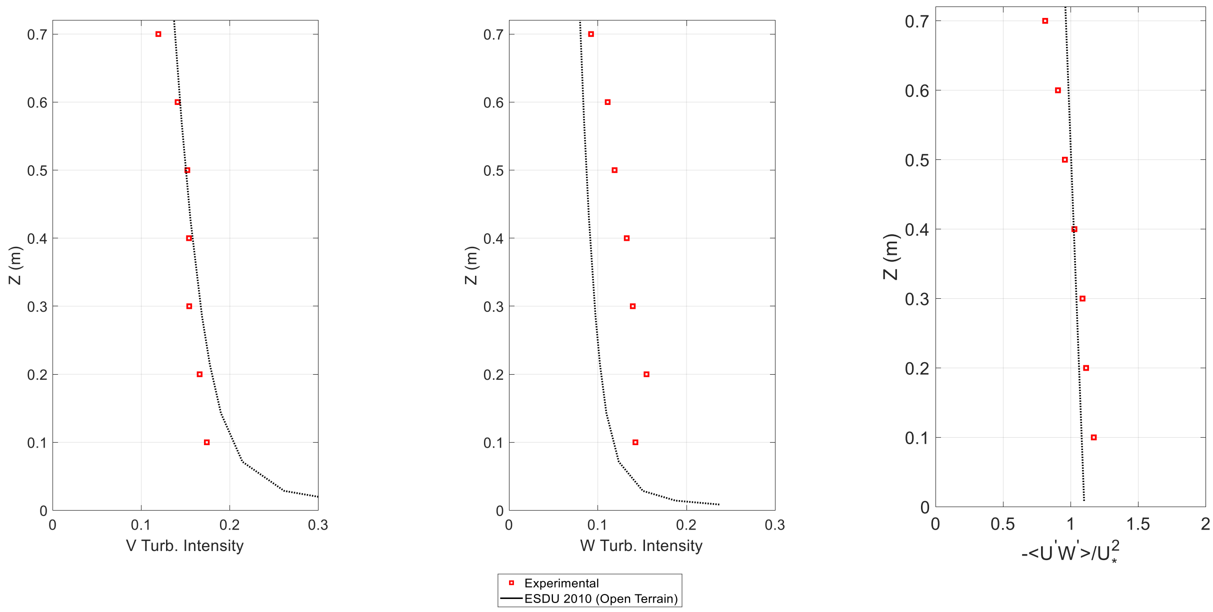

(c) I_v Turbulence intensity (d) I_w Turbulence intensity (e) <$u'w'$> Reynolds stress

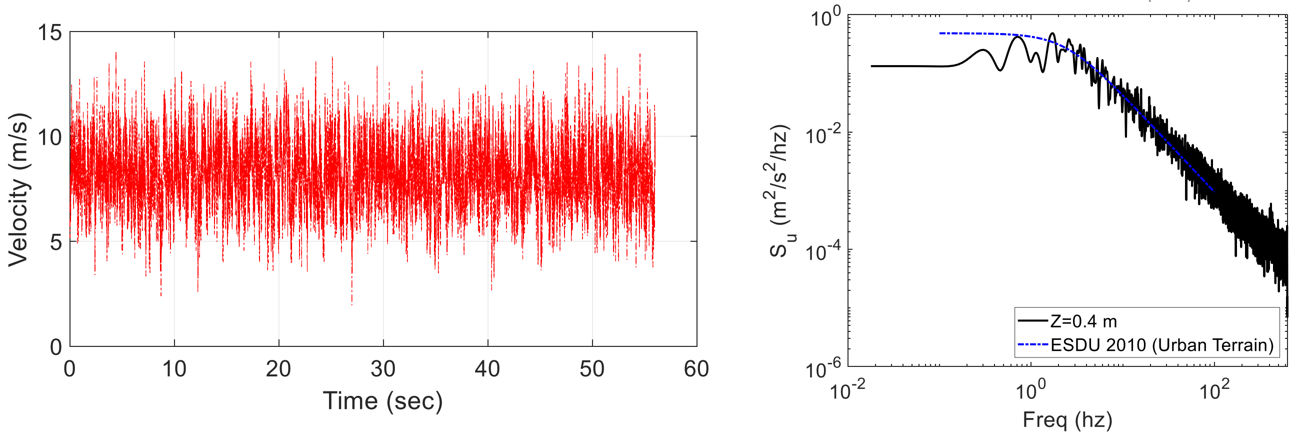

(f) Sample velocity time history at 0.4 m (g) PSD

Fig. 34 Wind field characteristics best matching urban terrain exposure at L_{scale} of 1:250 (R=70%)

achieve the best match was slightly higher than the blockage suggested from the CFD, however not very far. It can be seen also that the required blockage to achieve length scale of 1:250 is in general greater than blockage needed for the length scale of 1:500. Since the urban profile at the 1:250 (largest turbulence intensity) length scale was obtained at an effective blockage of only 70%, which is lower than the maximum blockage achievable by the system (i.e., 80%), it is expected that the system will work also with larger length scales which needs more turbulence.

6. Conclusions

In this study, a flow-conditioning system to model various Boundary Layers BLs for typical terrain conditions at the sub-sonic wind tunnel at Ryerson University was designed. The design was obtained using trial-and-error utilizing CFD LES of the wind tunnel with anticipated system. The design was obtained in three phases:

In phase I, effect of altering the turbulence generating elements: roughness blocks, spires, and slats (i.e., multi-level barriers) on the resulting BL was investigated. Mean velocity and turbulence intensity profiles of resulting BLs were compared with target profiles for open, suburban and urban terrains. It was found out that the case of 10 cm roughness blocks staggered over 6 columns (with a total number of 15 blocks) led to promising profiles close to the target but limited to half the tunnel depth. In order to extend the depth of the acceptable BLs, a system of truncated spires (covering the height of tunnel) with multi-level barriers (slats) was suggested and examined. It was found out that the system when equipped with tapered slats (varying from 8 cm at the floor to 2 cm at the top) with 40% blockage leads to well matching profiles with open terrain exposure. Since it is expected that rougher (i.e., suburban or urban) terrains can be generated by increasing the blockage, a slat-spire system (shown in Fig. 15) with two slat layers (one fixed and one movable) is suggested to allow for controlling the blockage between the range of 40 - 80%.

In phase II, the slat-spire system was tuned to successfully generate suburban and urban BLs. The system was constructed and experimentally validated at the wind tunnel in Phase III by comparing characteristics of the resulting flow field with the target characteristics based on the ESDU at two typical length scales (1:500 and 1:250). The system achieved a very good match with the target characteristics which prove the accuracy of the system and capability of generating accurate BL profiles for various terrain exposures.

Acknowledgements

The authors would like to thank Ryerson University for the funding of this project through the start-up and equipment grants of the third author. The authors are thankful to SHARCNET for the computational resources for the CFD simulations and for the folks at the WindEEE Research Institute at UWO for providing the Cobra probes for the experimental validation.

References

Aboshosha, H., Bitsuamlak, G. and El Damatty, A. (2015), "LES of ABL flow in the built-environment using roughness modeled by fractal surfaces", *Sustain. Cities Soc.*, **19**, 46-60. https://doi.org/10.1016/j.scs.2015.07.003.

Aboshosha, H., Ibrahim, A.M., El Damatty, A.A. and Hamada, A., (2016), "Dynamic behaviour of transmission lines structures under synoptic wind loads", *CIGRE-IEC Colloquium*, Canada.

Aly, A.M., Chowdhury, A.G. and Bitsuamlak, G. (2011), "Wind profile management and blockage assessment for a new 12-fan Wall of Wind facility at FIU", *Wind Struct*., **14**(4), 285-300.

AS/NZS 1170.2 (2010), "Australian/New Zealand standards, structural design actions - part 2, Wind Actions", Standards Australia International Ltd – Standards, New Zealand.

ASCE/SEI 7-16 (2016), "Minimum design loads for buildings and other structures", *Amer. Soc. Civil Eng*., ASCE, New York, U.S.A.

Barcelos, D. (2015), "Flow 1uality testing and improvement of the Ryerson university low speed wind tunnel", Master Thesis, Ryerson University, Canada.

BLWT Outline (2007), Wind Tunnel Testing: A general outline, Boundary Layer Wind Tunnel Laboratory.

Carroll, T.B. (2017). "A design methodology for rotors of small multirotor vehicles", Master thesis, Ryerson University, Canada.

Cermak, J.E. (2003), "Wind-tunnel development and trends in applications to civil engineering", *J. Wind Eng. Ind. Aerod*., **91**, 355-370.

Cheng, H. and Castro, I.P. (2002), "Near-wall flow development after a step change in surface roughness", *Bound. Lay. Meteorol*., **105**, 411-432. https://doi.org/10.1023/A:1020355306788.

Counihan, J. (1969), "A method of simulating a neutral atmospheric boundary layer in a wind tunnel", *AGARD Conference Proceedings 43*.

Counihan, J. (1969), "An improved method of simulating an atmospheric boundary layer in a wind tunnel", *Atmos. Environ. Pergamon Press*, **3**, 197-214. https://doi.org/10.1016/0004-6981(69)90008-0.

Counihan, J. (1973). "Simulation of an adiabatic urban boundary layer in a wind tunnel", *Atmos. Environ*., **7**, 673-689. https://doi.org/10.1016/0004-6981(73)90150-9.

Cui, W. and Caracoglia, L. (2017), "Examination of experimental variability in HFFB testing of a tall building under multi-directional winds", *J. Wind Eng. Ind. Aerod*., **171**, 34-49. https://doi.org/10.1016/j.jweia.2017.09.001.

Davenport, A. (1961), "A statistical approach to the treatment of wind loading on tall masts and suspension bridges", Ph. D. Dissertation. University of Bristol, U.K.

Davenport, A.G. (2002), "Past, present and future of wind engineering", *J. Wind Eng. Indus. Aerod*., **90**, 1371-1380. https://doi.org/10.1016/S0167-6105(02)00383-5.

De Paepe, W., Pindado, S., Bram, S. and Contino, F. (2016), "Simplified elements for wind-tunnel measurements with type-III-terrain atmospheric boundary layer", *J. Int. Measure. Confederation*, **91**, 590-600. https://doi.org/10.1016/j.measurement.2016.05.078.

Elawady, A., Aboshosha, H., El Damatty, A., Bitsuamlak, G., Hangan, H. and Elatar, A. (2017), "Aero-elastic testing of multi-spanned transmission line subjected to downbursts", *J. Wind Eng. Ind. Aerod*., **169**, 194-216. https://doi.org/10.1016/j.jweia.2017.07.010.

EN (2010), "European standard, Eurocode Part 1-4: general actions - wind actions", European Committee for Standardization.

Engineering Sciences Data Unit (2001), "Characteristics of atmospheric turbulence near the ground. Part II: Single point data for strong winds", London, U.K.

Engineering Sciences Data Unit (2002), "Strong winds in the atmosphericboundary layer. Part 1: Hourly-mean wind speeds", London, U.K.

Engineering Sciences Data Unit (2010), "Characteristics Of atmospheric turbulence near the ground, Part I: definitions and general information", *Eng. Sci. Data Unit* 74030. London, U.K.

Eric Ho, T., Surry, D. and Davenport, A.G. (1990), "The variability of low building wind loads due to surrounding obstructions", *J. Wind Eng. Ind.. Aerod*., **36**, 161-170. https://doi.org/10.1016/0167-6105(90)90301-R.

Farell, C. and Iyengar, A.K. (1999), "Experiments on the wind tunnel simulation of atmospheric boundary layers", *J. Wind Eng. Ind. Aerod*., **79**, 11-35. https://doi.org/10.1016/S0167-6105(98)00117-2.

Ge, Yaojun and Zhao, Lin. (2014), "Wind-excited stochastic vibration of long-span bridge considering wind field parameters during typhoon landfall", *Wind Struct*., **19**(4), 421-441. https://doi.org/10.12989/was.2014.19.4.421.

Germano, M., Piomelli, U., Moin, P. and Cabot, W. (1991), "A dynamic subgrid-scale eddy viscosity model", *Phys. Flu*., **3**(7), 1760-1765. https://doi.org/10.1063/1.857955.

Han, Y., Chen, Z.Q. and Hua, X.G. (2010), "New estimation methodology of six complex aerodynamic admittance functions", *Wind Struct*., **13**(3), 293-307.

Holmes, J.D. (2014), "Along- and cross-wind response of a generic tall building: Comparison of wind-tunnel data with codes and standards", *J. Wind Eng. Ind. Aerod*., **132**, 136-141. https://doi.org/10.1016/j.jweia.2014.06.022.

Hui, Y., Tamura, Y. and Yang, Q. (2017), "Analysis of interference effects on torsional moment between two high-rise buildings based on pressure and flow field measurement", *J. Wind Eng. Ind. Aerod*., **164**, 54-68. https://doi.org/10.1016/j.jweia.2017.02.008.

Irwin, H. (1981), "The design of spires for wind simulation", *J. Wind Eng. Ind. Aerod*., **7**, 361-366.

Irwin, P., Dragoiescu, C., Cicci, M. and Thompson, G. (2012), "Wind tunnel model studies of aerodynamic lifting of roof pavers", *Proceedings of ATC & SEI Conference on Advances in Hurricane Engineering 2012*. Florida, October.

Ishizaki, H. and Nishimura, H. (1992), "Wind tunnel experiments on the vibrations of flexible models of a tall building", *J. Wind Eng. Ind. Aerod*., **42**(1-3), 1065-1072. https://doi.org/10.1016/0167-6105(92)90113-O.

Isyumov, N. (2012), "Alan G. Davenport's mark on wind engineering", *J. Wind Eng. Ind. Aerod*., **104-106**, 12-24. https://doi.org/10.1016/j.jweia.2012.02.007.

Jubayer, C., Elatar, A. and Hangan, H. (2016), "Pressure distributions on a low-rise building in a laboratory simulated downburst", *8th International Colloquium on Bluff Body Aerodynamics and Applications*. Boston, U.S.A. June.

Jubayer, C.M. and Hangan, H. (2016), "A numerical approach to the investigation of wind loading on an array of ground mounted solar photovoltaic (PV) panels", *J. Wind Eng. Indus. Aerod*., **153**, 60-70. https://doi.org/10.1016/j.jweia.2016.03.009.

Jubayer, C.M. and Hangan, H. (2018), "A hybrid approach for evaluating wind flow over a complex terrain", *J. Wind Eng. Ind. Aerod*., **175**, 65-76. https://doi.org/10.1016/j.jweia.2018.01.037.

Kim, W., Tamura, Y. and Yoshida, A. (2015), "Interference effects on aerodynamic wind forces between two buildings", *J. Wind Eng. Ind. Aerod*., **147**, 186-201. https://doi.org/10.1016/j.jweia.2015.10.009.

Kim, Y.C., Yoshida, A. and Tamura, Y. (2013), "Influence of surrounding buildings on wind loads acting on low-rise building", *J. Struct. Eng*., **139**(2), 275-283. https://doi.org/10.1061/(ASCE)ST.1943-541X.0000625.

Kozmar, H. (2011), "Truncated vortex generators for part-depth wind-tunnel simulations of the atmospheric boundary layer flow", *J. Wind Eng. Ind. Aerod*., **99**(2-3), 130-136. https://doi.org/10.1016/j.jweia.2010.11.001.

Li, B., Yang, Q., Solari, G. and Wu, D. (2018), "Investigation of wind load on 1,000 m-high super-tall buildings based on HFFB tests", *Struct. Health Monit*., **25**(2). https://doi.org/10.1002/stc.2068.

Li, Q.S., Wu, J.R., Liang, S.G., Xiao, Y.Q. and Wong, C.K. (2004), "Full-scale measurements and numerical evaluation of wind-induced vibration of a 63-story reinforcedconcrete tall building", *Eng. Struct*., **26**(12), 1779-1794. https://doi.org/10.1016/j.engstruct.2004.06.014.

Liu, L., Zhang, L., Wu, B. and Chen, B. (2017), "Numerical and experimental studies on grid-generated turbulence in wind tunnel", *J. Eng. Sci. Technol. Rev*., **10**(3), 159-169.

Loredo-Souza, A. and Davenport, A. (1998), "The effects of high winds on transmission lines", *J. Wind Eng. Ind. Aerod*., **74-76**(1), 987-994. https://doi.org/10.1016/S0167-6105(98)00090-7.

Loredo-Souza, A. and Davenport, A. (2001). "A novel approach for wind tunnel modelling of transmission lines", *J. Wind Eng. Ind. Aerod*., **89(**11-12), 1017-1029. https://doi.org/10.1016/S0167-6105(01)00096-4.

Loredo-Souza, A. and Davenport, A. (2002), "Wind tunnel aeroelastic studies on the behaviour of two parallel cables", *J. Wind Eng. Ind. Aerod*., **90**(4-5), 407-414. https://doi.org/10.1016/S0167-6105(01)00211-2.

Ma, T.T.; Zhao, L. and Cao, S.Y. (2013), "Investigations of aerodynamic effects on streamlined box girder using two-dimensional actively-controlled oncoming flow", *J. Wind Eng. Ind. Aerod*., **122**, 118-129. https://doi.org/10.1016/j.jweia.2013.07.011.

Mooneghi, M.A., Irwin, P. and Chowdhury, A.G. (2014), "Large-scale testing on wind uplift of roof pavers", *J. Wind Eng. Ind. Aerod*., **128**, 22-36. https://doi.org/10.1016/j.jweia.2014.03.001.

NBCC (2015), "The National Building Code of Canada", National Research Council. Ottawa, Canada.

Nguyen, C.H., Freda, A., Solari, G. and Tubino, F. (2015), "Aeroelastic instability and wind-excited response of complex lighting poles and antenna masts", *Eng. Struct*., **85**(15), 264-276. https://doi.org/10.1016/j.engstruct.2014.12.015.

Nguyen, C.H., Freda, A., Solari, G. and Tubino, F. (2015), "Experimental investigation of the aeroelastic behavior of a complex prismatic element", *Wind Struct*., **20**(5), 683-699. http://dx.doi.org/10.12989/was.2015.20.5.683.

Perera, M. 1(978), "A wind tunnel study of the interaction between along-wind and cross-wind vibrations of tall, slender structures", *J. Wind Eng. Ind. Aerod*., **3**(4), 315-341. https://doi.org/10.1016/0167-6105(78)90036-3.

Piccardo, G. and Solari, G. (1998), "Closed form prediction of 3-D wind-excited response of slender structures", *J. Wind Eng. Ind. Aerod.*, **74-76**(1), 697-708. https://doi.org/10.1016/S0167-6105(98)00063-4.

Pires, L.B. M. *et al*., (2013), "Simulations of the atmospheric boundary layer in a wind tunnel with short test section", *J. Aeros.Technol. Manage*., **5**(3), 305-314.

Refan, M. and Hangan, H. (2016), "Characterization of tornado-like flow fields in a new model scale wind testing chamber", *J. Wind Eng. Ind. Aerod*., **151**, 107-121. https://doi.org/10.1016/j.jweia.2016.02.002.

Robins, A. (1979), "The development and structure of simulated neutrally stable atmospheric boundary layers", *J. Wind Eng. Ind. Aerod*., **4**, 71-100. http://pascal-francis.inist.fr/vibad/index.php?action=getRecordDetail&idt=PASCAL7930139170.

Salizzoni, P., Soulhac, L., Mejean, P. and Perkins, R.J. (2008), “Influence of a two-scale surface roughness on a neutral turbulent boundary layer”, *Bound. Lay. Meteorol.*, **127**, 97-110. https://doi.org/10.1007/s10546-007-9256-8.

Schultz, M., Schatzmann, M. and Leitl, B. (2005), “Effect of roughness inhomogeneities on the development of the urban boundary layer”, *Int. J. Environ. Pollut.*, **25**, 105-117. https://doi.org/10.1504/IJEP.2005.007659.

Shojaee, S.M.N., Uzol, O. and Kurc, O. (2014), “Atmospheric boundary layer simulation in a short wind tunnel”, *Int. J. Environ. Sci. Technol.*, **11**(1), 59-68. https://doi.org/10.1007/s13762-013-0371-4.

Smagorinsky, J. (1963), “General circulation experiments with the primitive equations: I. the basic experiment”, *Mon. Weather Rev.*, **91**(3), 99-164. https://doi.org/10.1175/1520-0493(1963)091%3C0099:GCEWTP%3E2.3.CO;2.

Solari, G., Pagnini, L. and Piccardo, G. (1997), “A numerical algorithm for the aerodynamic identification of structures”, *J. Wind Eng. Ind. Aerod.*, **69-71**, 719-730. https://doi.org/10.-6105(97)00200-6.

Sun, X., Liu, H., Su, N. and Wu, Y. (2017), “Investigation on wind tunnel tests of the Kilometer skyscraper”, *Eng. Struct.*, **148**(1). 340-356. https://doi.org/10.1016/j.engstruct.2017.06.052.

Tamura, Y., Kim, Y.C., Tanaka, H., Bandi, E.K., Yoshida, A. and Ohtake, K. (2013), “Aerodyanmic and response characteristics of super-tall buildings with various configurations”, *Proceedings of the Eighth Asia-Pacific Conference on Wind Engineering*, India, December.

Tamura, Y., Xu, X., Tanaka, H., Kim, Y.C., Yoshida, A. and Yang, Q. (2017), “Aerodynamic and pedestrian-level wind characteristics of super-tall buildings with various configurations”, *Proceedings of the 10th International Conference on Structural Dynamics*, Italy, September.

Tanaka, H. and Davenport, A.G. (1983), “Wind-enduced response of golden gate bridge”, *J. Mech.*, **109**(1), 296-312. https://doi.org/10.1061/(ASCE)0733-9399(1983)109:1(296).

Varshney, K. (2012), “Tailoring wind properties by various passive roughness elements in a boundary-layer wind tunnel”, *J. Therm. Sci.*, **21**(4), 336-341.

Vita, G., Hemida, H., Andrianne, T. and Baniotopoulos, C.C. (2018), “Generating atmospheric turbulence using passive grids in an expansion test section of a wind tunnel”, *J. Wind Eng. Ind. Aerod.*, **178**, 91-104. https://doi.org/10.1016/j.jweia.2018.02.007.

AD